Assessing nanotoxicity of food-relevant particles: A comparative analysis of cellular responses in cell monolayers versus 3D gut epithelial cultures

Archana Gautam[1 #], Hui Kheng Lim[2,3,4 #], Jasmine Jia'En Li[5 #], Christopher Owen Hughes[2,3,4], Calvin Wee Sing Yeo[5], Moumita Rakshit[1], David Ian Leavesley[3], Michelle Jing Sin Lim[4,6], Joseph Choon Wee Tan[4], Li Yi Tan[1], Joanne Sheot Harn Chan[5], Benjamin Paul Chapman Smith[2,4,6,7 *], Kee Woei Ng[1,3,8 **]

[1]School of Materials Science and Engineering, Nanyang Technological University, 50 Nanyang Avenue, Singapore

[2]Innovations in Food and Chemical Safety (IFCS) Programme, Agency for Science, Technology and Research, Singapore

[3]Skin Research Institute of Singapore (SRIS), Agency for Science, Technology and Research, Singapore

[4]Future Ready Food Safety Hub (a joint initiative of A*STAR, SFA & NTU), Nanyang Technological University, Singapore

[5]National Centre for Food Science, Singapore Food Agency, Singapore

[6]Singapore Institute of Food and Biotechnology Innovation (SIFBI), Agency for Science, Technology and Research, Singapore

[7]Chemical Senses Center, 3500 Market Street, Pennsylvania, 19104, USA

[8]Nanyang Environment and Water Research Institute, Nanyang Technological University, 1 Cleantech Loop, CleanTech One, Singapore

[#] These authors contributed equally to this work

Corresponding authors:

*bsmith@monell.org

**kwng@ntu.edu.sg

Abstract

Engineered nanoparticles (NPs) are extensively used in the food industry, yet safety concerns remain. The lack of validated methodologies is a bottleneck towards resolving this uncertainty. Hence, the current study aims to compare two cell models by examining the toxicological impacts of two food-relevant NPs (SiO_2 and Ag) on intestinal epithelia using monolayer Caco-2 cells and full-thickness 3D tissue models of human small intestines (EpiIntestinal™). Comprehensive characterization and dosimetric analysis of the NPs were performed to determine effective doses and model realistic exposures. Neither genotoxicity nor cytotoxicity were detected in the 3D tissues after NP treatment, while the 2D cultures exhibited cytotoxic response from Ag NP treatment for 24 hr at 1 μg/ml. Hyperspectral imaging and transmission electron microscopy confirmed uptake of both NPs by cells in both 2D and 3D culture models. Ag NPs caused an increase in autophagy, whereas SiO_2 NPs induced increased cytoplasmic vacuolization. Based on realistic exposure levels studied, the 3D small intestinal tissue model was found to be more resilient to NP treatment compared to 2D cell monolayers. This comparative approach towards toxicological assessment of food relevant NPs could be used as a framework for future analysis of NP behavior and nanotoxicity in the gut.

Keywords: Nanoparticles, nanotoxicology, intestine, genotoxicity, 3D models

1.0 Introduction

The rapid advancement in nanotechnology, in the recent years, have paved the way for the development of innovative nanomaterials, particularly within the realm of food science. Today, the majority of our food products are enriched with various food-based additives intentionally incorporated to extend their shelf-life, enhance safety, freshness, taste, texture and appearance, as highlighted by the World Health Organization[1]. Significantly, researchers have revealed that a substantial portion of these approved food additives exists in nano-sized forms, underscoring the pervasive integration of engineered nanomaterials in the food industry. These nanomaterials play a pivotal role in elevating the overall food quality, flavor, shelf life, aesthetics, and nutritional value of food products. Furthermore, they have become indispensable in the development of next-generation food contact materials. Their unique physio-chemical properties contribute to improved barrier properties in food packaging and they serve as sensors for food quality and freshness indicators[2]. However, the widespread incorporation of nanomaterials into foods and food contact materials has prompted concerns regarding their potential impact on human health[3].

Consumers are exposed to NPs through ingestion of NPs-containing food products or beverages, ingestion being the third route of exposure, after dermal and inhalation[4,5]. Silicon Dioxide (SiO_2) NPs are among the most widely used NPs and a registered food additive E551 in the European Union. They are used as an anti-caking agent[6,7] in powdered or granulated materials to prevent clumping, and as a carrier, thickener, and color diluent in products such as confectionaries, powdered mixtures, and seasonings[8]. Reports show the presence of silica NPs in food products with a diameter between 10 and 50 nm[9]. Additionally, their size could be further reduced during the digestion process and modification of their aggregation state on contact with the biological fluids[10]. Silica NPs in food prepared with E551 additive was

reported to be present after intestinal digestion suggesting that upon consumption of foods containing E551, the gut epithelium is most likely exposed to nano-size silica[11]. Previous research highlights that these NPs possess the ability to easily penetrate the cell membranes, interacting with human cells and tissues, raising potential health risks given their inherent characteristics[12]. Likewise, the literature contains a wealth of studies examining the intestinal toxicity of silica NPs, including those found in the E551 additive where they have been reported to cause injuries to cells, tissues, and organs in vitro and in vivo[13–15].

Silver (Ag) NPs are known to possess antimicrobial and antioxidant properties and they have been used as antimicrobial agents in foods and food packaging materials[16]. While they can inhibit biofilm formation and browning in fresh cut fruits it is possible that some of these NPs may migrate from these packaging materials into the foods so that they could be ingested by humans. The addition of Ag NPs into food packaging can also improve their barrier and mechanical properties[17]. At present, there is still limited information on the potential toxicity of Ag NPs ingested with foods, with some studies reporting no toxicity and others reporting appreciable toxicity in humans[16]. Numerous animal studies have reported that dietary intake of Ag NPs caused lymphocyte infiltration, pigmentation of villi, discharge of mucus granules and abnormal mucus composition in the intestine. Animal studies have further reported that these NPs can accumulate in various organs after ingestion, including the liver, kidneys, spleen, stomach, and small intestine[18]. However, it is not clear whether these NPs have toxic effects when consumed by humans in the levels which are close to those actually achievable through food consumption. Specific to genotoxic effects of both SiO_2 and Ag NPs, contradictory reports are found in the literature [19,20]. Comparing across the literature presents significant challenges primary because of non-harmonized methodologies.

Nevertheless, these studies are fraught with significant limitations. Typically, the NPs were incubated with intestinal cell lines, predominantly Caco-2, without accounting for the presence of an epithelial barrier in the real tissue, and the mucus layer. This barrier serves as the first line of defense against invasion of foreign microorganisms, including NPs. Hence, based on the facts reported in these studies, synthetic food additives in the food industry needs to be reexamined in a more realistic model, along with their physiochemical properties fully characterized so that the safety level for human intake can be entirely revealed. Therefore, to overcome these drawbacks, our study takes a pioneering approach, addressing these limitations through the implementation of a 3D intestinal epithelial model for a more comprehensive evaluation of toxicity. This study focuses on investigating the impact of two extensively utilized food-grade NPs, SiO_2 (E551) and Ag (AGCO75), using both traditional 2D cell cultures and advanced 3D intestinal epithelial models. Our comprehensive evaluation encompasses their characteristics, solubility, cytotoxicity, cellular uptake and localization, as well as genotoxicity. By delving into these aspects, we aim to provide valuable insights into the potential risks associated with these commonly employed food-based NPs, contributing to the ongoing discourse on their responsible use in the food industry.

Effectively all cells in the body are organized and resided in a well-organized 3D environment with extensive cell-cell and cell-matrix interactions, which is essential for their growth and metabolism[21]. 2D cell cultures do not adequately recapitulate the appropriate level of in vivo cellular responses because cell–cell and cell–matrix interactions are markedly reduced in the monolayer cell culture raised on a flat culture dish[22]. Though providing valuable information, tests performed with 2D monolayer cultures do not always accurately predict actual toxicity of in vivo conditions due to the absence of key biological and physiological processes[23]. The gut makes up a large portion of the body's external surface[24] and the small intestine is where

around 90% of the digestion and absorption of food occurs[25]. Thus, it is a major exposure site of ingested toxicants. Whilst 3D models can lack consistency due to variabilities across multiple factors[26] , the production of EpiIntestinal™ microtissues are highly standardized and validated as a representative in vitro mimicry system with structural, biochemical, physiological, functional, and mechanistic properties highly resembling the human gut[27]. When use in food hazard identification, this model offers site-of-first contact information of ingested material. Unlike spheroids or organoids which have issues with NPs penetration, the upward facing luminal structure (apical side) of EpiIntestinal™ microtissues allows homogenous exposure to NPs. It is worth noting that loss of tissue barrier integrity is the first indication of any dysfunction or damage to intestinal epithelium. Assessment of barrier function is permissible due to the accessibility to intestinal luminal surfaces. EpiIntestinal™ microtissues can be cultured for an extended period of time up to 28 days[28], which allows multiple dosing and long-term studies. Furthermore, the EpiIntestinal™ model is commercially available and can be readily sourced in Europe, the US and Asia, making it a valuable model for use in both research and regulatory studies. However, like many other in vitro models, the lack of intestinal peristalsis, digestive fluid, mucous layer and microflora are limitations[26].

2.0 Materials and Methods

2.1 Chemicals

All chemicals were obtained from Sigma Aldrich unless otherwise specified.

2.2 Nanoparticle characterization

SiO_2 (Harvard repository, USA), and Ag NPs (Nanocomposix, USA) were characterized for their pristine size and morphology using a transmission electron microscope (TEM JEOL 2010 HR & UHR) at an accelerating voltage of 200 kV. The elemental composition of NPs was further identified by Energy Dispersive Spectroscopy (EDS; EDAX, USA) mediated compositional analysis.

2.3 Determination of $DSE_{(CRIT)}$

The critical delivered sonication energy (DSE_{CRIT}), which is the minimum required energy per dispersion volume (J/ml) to achieve the smallest possible agglomerates, was determined for each NP type by incremental sonication and size characterization. Suspensions of the NPs in deionized (DI) water were dispersed using a probe sonicator that was first calibrated to determine its energy delivery rate (i.e., Js^{-1}). The mean hydrodynamic diameter of the suspension over time was measured by dynamic light scattering (DLS) and plotted to determine the minimum sonication time and thus energy required to achieve the smallest possible diameter agglomerates. All measurements were performed in triplicate, at 25 °C, using disposable optical polystyrene micro-cuvettes.

2.4 NPs Solubility

NPs suspension (15 mg/ml) were prepared by sonication at DSE_{CRIT} and diluted to 1 mg/ml concentration in water, 3D EpiIntestinal™ tissue medium (SMI-100) and Dulbecco's modified eagle medium (DMEM). The suspensions were incubated at 37°C under ambient conditions for 24 hours, following which any undissolved NPs were removed using high speed centrifugation (25000 g, 15 mins) followed by filtration through a 0.25 µm pore size filter

(Merck Millipore, USA), prior to Inductively Coupled Plasma Optical Emission Spectrometry (ICP-OES) analysis. This was followed by quantification of the amount of dissolved ions.

2.5 Dosimetry

The In vitro Sedimentation, Diffusion and Dosimetry (ISDD) model was followed for performing particle dosimetry [29,30]. The effective density was derived using the volumetric centrifugation method described by DeLoid et al: 1 ml of 1 mg/ml suspension of NPs in SMI-100 and DMEM was kept in packed cell volume (PCV) tubes (Techno Plastic Products (TPP), Trasadingen, Switzerland) and centrifuged in bench-top swing-out rotor centrifuge at 2000g for 1 hour[31]. From the pellet obtained, the volume of the agglomerate pellet (V_{pellet}) was measured with the help of a slide-rule-like easy measure device which was also provided by the PCV tube manufacturers. The Vpellet value was used to determine the effective density (ρEV) using Equation (1) as follows:

$$\rho EV = \rho media + [\left(\frac{Menm}{Vpellet\ .\ SF}\right)\left(1 - \left(\frac{\rho Media}{\rho ENM}\right)\right] \quad (1)$$

where ρmedia is the density of media, Menm is the mass of NPs, Vpellet is the volume of the pellet, SF is the stacking factor and ρENM is the density of pristine NPs. The effective density was calculated for the test NPs in SMI-100 and MEM. Using this effective density, the fraction of particles sedimented (fD) over different time period was determined via MATLAB simulation. fD was then used to calculate the time weighted average dosage.

2.6. *In vitro* cell and tissue culture

(i) 2D cell culture

Caco-2 cell lines, purchased commercially (HTB-37™, American Type Culture Collection ATCC, Manassas, VA) were maintained in complete media MEM supplemented with L-glutamine and 20% fetal bovine serum in 37°C, 5% CO_2. Cells were cultured for at least 2 passages after initiation from liquid nitrogen storage before assay use.

(ii) 3D tissue culture

3D EpiIntestinal™ tissue (SMI-200-FT v2.0) was purchased from MatTek Corporation® (Ashland, MA). The model incorporates enterocytes, paneth cells, M cells, tuft cells and intestinal stem cells into a highly differentiated, polarized epithelium, as described in detail elsewhere[32]. The tissues were processed as instructed by the supplier, treated with test NPs at the concentrations reported in the Results section and maintained with SMI-100-MM culture media at the air-liquid interface at 37°C, 5% CO_2/95% air and 98% relative humidity.

2.7 Tissue barrier integrity assessment

3D intestinal tissues were apically treated with test materials every 24 hours, for a total of 72 hours, prior to assessment of barrier integrity.

FITC-dextran tissue permeability assay:

Changes induced to the barrier function of the EpiIntestinal™ tissues were monitored using fluorescein isothiocyanate (FITC)-dextran 20 kDa (FD20, Sigma Aldrich, St Louis, MO) tissue permeability assay. The tissue permeability was measured in EpiIntestinal™ tissues after adding 3 mg/ml of FD20 to the apical culture media and incubating at 37˚C, for 2h in 5% CO_2/95% air. Tissue permeability was calculated based on the measured Fluorescence Intensity (FI) of FD 20 in the basolateral medium compartment of the 3D cultures, using a microplate reader (Envision, Perkin Elmer, Waltham, MA) at 485/530 nm. FD20 permeation

from the donor medium to the receiver medium was normalized to FD20 that permeated through blank inserts, using Equation (2) as follows:

$$Tissue\ Permeability\ (\%) = \frac{FI\ (basolateral, Tissue) - FI\ (Blank)}{FI\ (basolateral, Blank) - FI\ (Blank)} \times 100 \quad (2)$$

where, *FI (basolateral, Tissue)* represents the measured FD20 fluorescence intensity in the basolateral compartment of the tissue-containing wells; *FI (basolateral, Blank)* represents the measured FD20 fluorescence intensity in the basolateral compartment of the blank inserts; *FI (Blank)* represents the background fluorescence of the medium alone. Tissue barrier integrity was considered uncompromised if FD20 permeability was less than 4%.

Transepithelial electrical resistance (TEER) measurement:

Changes in barrier integrity of the EpiIntestinal™ tissues were assayed using *TEER* with an EVOM volt-ohmmeter equipped with an EndOhm electrode chamber (World Precision Instruments, Sarasota, FL), according to the manufacturer's published protocols. Raw resistance values (Ω) were converted to TEER readings (Ω*cm^2) by multiplying the raw measurements of each tissue by the surface area of the cell culture inserts (0.6 cm^2).

2.8 Tissue dissociation

3D intestinal tissues were dissociated using human tumour dissociation kit (Miltenyl Biotec, Bergisch Gladbach, Germany), as per manufacturers' instruction, with minor modifications. Individual 3D tissues were excised from the culture inserts and incubated for 15 min in cell recovery solution (Corning, Tewksbury, MA). The tissues were subsequently peeled off from

the membrane with fine point forceps. The peeled tissues were placed into gentle MACS C-tube (Miltenyi Biotech, Bergisch Gladbach, Germany) containing the enzyme mix described in the kit's protocol. The tubes were then transferred into a gentleMACS octo dissociator with heater (Miltenyi Biotech, Bergisch Gladbach, Germany), and subjected to one cycle of '37C_m_LPDK_1' program. Upon completion, the cell suspension was centrifuged at 1000 rpm for 5 min; the supernatant was removed, and the pellet was resuspended in 2 ml of Hanks Balanced Salts Solution (HBSS) +Ca/Mg. Total cell number was estimated through cell counting with hemocytometer. The cells were then fixed for micronuclei cytome scoring.

2.9 Micronucleus (MN) cytome assay in 3D EpiIntestinal™ tissue

The MN cytome assay, RICyt, was performed as reported earlier[33]. Tissues were repeatedly exposed to test substances over a period of 10 days, harvested and dissociated into single cell suspension as described above. Cell suspension samples was fixed in Carnoy's solution with 3 fixation steps in methanol/acetic acid 16:1, supplemented with 4% v/v formaldehyde. The cell suspension was aged at least overnight at 4°C to improve the quality of fixed cells. The fixed cells were stained with acridine orange and immediately scored. Cells were scored per criteria originally described by Tolbert *et al*.[34] and Thomas *et al*.[35] One thousand total cells were scored per microtissue to determine the frequency of MN and cytome. The percentage of MN and cytome at each concentration of test chemical was compared with the solvent control. The results were generated from three independent experiments. Each experiment consisted of a single microtissue per dose.

2.10 Comet assay in *in vitro* 3D EpiIntestinal™ tissue

Comet assay was performed as described by Hughes et al[36]. In brief, the apical media was replaced with fresh media containing test materials of interest dispersed in solvent. Tissues were incubated for 24 hours before they were again rinsed and replenished with fresh apical media containing test material. 21 hours after first exposure, tissues were rinsed and dosed again for a final 3 hours before harvesting for comet assay. The total treatment time was 48 hr. At end of exposure, tissues were dissociated and isolated cells were mixed with low melt agarose (LMA) then transferred to each of the two spots on agarose pre-coated glass slides. Slides were cooled to allow LMA to solidify. Cell lysis was carried out by incubating the slides in pre-chilled lysis buffer. For DNA unwinding, slides were then incubated in alkali DNA unwinding solution at room temperature for 20 minutes and electrophoresis was carried out for 30 minutes at 21 V (1V/cm) in electrophoresis buffer using an electrophoresis chamber (4250-050-ESK, Trevigen, Gaithersburg, MD). The electrophoresis tank and solution were pre-chilled for several hours in a cold room prior to usage and electrophoresis was performed in cold room conditions. After electrophoresis, slides were immediately neutralized in distilled water and then twice further for 10 minutes, before being dehydrated in ethanol. Slides were then left to dry overnight at room temperature. DNA was stained with SYBR Green, excess stain was removed and slides were left to dry before they were ready for analysis. Samples were scored and analyzed using a Metafer v3.13.3 scoring platform (Metasystems, Germany). DNA damage was measured and reported as median % tail DNA per microtissue, a minimum of 100 viable comets per tissue. The results for comet assay were generated from three independent experiments. Each experiment consisted of a single microtissue per test concentration.

2.11 Micronucleus assay in Caco-2 cell line

For each treatment assay, cells were seeded at a seeding density of 2 x 10^5 cells/dish in 60mm culture dishes and for 24 h prior to exposure of test materials in MEM with 5% FBS. Each treatment was repeated in duplicates. Caco-2 cells were incubated with the test materials for 24 h and at the end of the treatment, the cells were gently washed twice in PBS and treated with 4.5 µg/ml cytochalasin B (cyto B; Wako Chemicals, Fujifilm) for 29 h. Following which, the cells were washed twice in PBS and replaced with fresh culture media containing 20% FBS for a recovery period of 1.5 h. Cells were then harvested with 0.25% trypsin-EDTA, exposed to cold hypotonic solution (75 mM KCl) and immediately centrifuged to collect the cell pellet. Cells were then resuspended and fixed first in fixative solution of cold methanol/acetic acid (3:1 [v/v]) diluted 1:1 in MEM culture media (20% FBS) and subsequently in undiluted fixative solution. Cells were centrifuged at 1000 rpm for 8 mins after each fixation step. Finally, cells were resuspended in the fixative solution and stored at 4°C. For slide preparations, the cells were spread onto clean glass slides and heat fixed at 51°C on a hot plate for 15 mins. After heat fixing, the cells were stained in 40 µg/ml acridine orange solution and analysed under fluorescence microscope. Micronuclei was performed according to criteria set out in OECD guidelines TG487. Results were taken from 3 independent assay runs.

2.12 Hyperspectral Imaging

Hyperspectral images were obtained and analyzed using the CytoViva® hyperspectral imaging (HSI) microscopy system coupled with the environment for visualizing images (ENVI) software. Spectral acquisition, HSI recording, and spectral mapping analysis were performed according to the Cytoviva® hyperspectral user manual. Prior to HSI analysis of the tissue samples, SiO_2 and Ag NPs were drop casted onto separate slides and mounted with a glass cover slip for HSI acquisition to create individual spectral libraries (SL). After which, HSI images

were recorded for non-treated and treated tissue samples. The spectral angle mapper (SAM), a classification algorithm, was applied to the HSI scans to map spectral similarities between the SLs of SiO_2/Ag NPs and tissue HSI scans. The SAM classification creates two output images: the SAM image of the tissue highlights the pixels that are matched with the applied SL, while the Rule image depicts how each pixel of the input image matches the endmember spectrum in grey scale.

2.13 Tissue sectioning and visualization by transmission electron microscopy (TEM)

To evaluate the localization of the NPs inside the cellular organelles, TEM was carried out. Briefly, the treated and untreated cells and tissues were fixed with a mixture of 4% paraformaldehyde and 2% glutaraldehyde solution overnight at room temperature (RT). They were post-fixed with 2% osmium tetroxide (Sigma Aldrich, USA) for 1 hour and washed with PBS to remove the fixative. Dehydration of cells was done with an ascending series of ethanol (25%, 50%, 75%, 95%, 100%) and pure acetone (100%) for 15 min each at RT. The cells and tissues were then infiltrated with a mixture of epoxy resin (Araldite 502 kit, Ted Pella, USA) and acetone at the ratio 1:1 for 30 min and 1:6 overnight. Each cell pellet and tissue were embedded in fresh resin within a polyurethane mould and polymerized for 48 hours at 60°C. The resulting resin-embedded cell capsules were sectioned at a thickness of 80–100 nm with an ultramicrotome and collected on copper grids. The sections were stained with 2% uranyl acetate for 8 min and lead citrate for 2-3 min before imaging (TEM JEOL 2010 HR & UHR) at an accelerating voltage of 200 kV.

2.14 Statistical Analysis

All quantitative results are presented as mean ± SD and represent a minimum of three independent experiments of n=3, unless otherwise stated. Comparison of means between two sample groups was determined by the two-tailed, unpaired Student's t-test while that for more than two sample groups was done with two tailed one-way ANOVA, and differences are considered significant if $p < 0.05$.

3.0 Results

3.1 Characterization of NPs

The electron micrographs of SiO_2 and Ag NPs are shown in Figure 1. The pristine sizes of the SiO_2 and Ag NPs are 22.1 ± 4.6 nm and 80.1 ± 8.3 nm, respectively, based on image analysis of TEM micrographs. EDX analysis, performed to verify the purity of these NPs, indicated the presence of well-defined elemental peaks for each NPs. Carbon and Copper peaks were detected due to the use of copper grids with lacey carbon for imaging. In addition to the pristine sizes, the hydrodynamic size of SiO_2 NPs was also examined in water (Figure 2A). The critical delivered sonication energy (DSE_{CRIT}) of SiO_2 NPs, was determined to be 235 J/ml. The calculated values for DSE for the different configurations of sonication and time for 15 ml NPs suspension are shown in supplementary Table 1. Sonicating the NPs at their DSE_{CRIT} would provide material-specific amount of acoustic power to break down particle agglomerates at the smallest and most uniform possible hydrodynamic size distribution[37], which allows the stabilization of these NPs in the different cell culture media used in the subsequent in vitro studies. This stabilization was evidenced from the dynamic light scattering (DLS) analysis that recorded NPs hydrodynamic size distribution and poly-dispersity indices, which remain relatively unchanged up to 10 days post dispersion in water (Figure 2B). Additional dispersion

step was not needed for Ag NPs as these were supplied as a fully dispersed solution in citrate buffer.

3.2 Examining the ionic solubility of SiO_2 and Ag NPs in water and tissue culture media

The dissolution both NPs were investigated in water and different culture media – SMI-100 and MEM at concentrations ranging from 1 ppm to 500 ppm (Figure 3). SiO_2 NPs showed very low levels of solubility in water (<1%), but increased dissolution (~30%) in SMI-100 and MEM media at up to 100ppm administered concentration. Ag NPs showed significantly higher dissolution at about 25% in water, 45% in SMI-100 and 55% in MEM media, over the same administered concentration range.

3.3 Dosimetric analysis

The effective densities for both NPs in different culture media were measured using the volumetric centrifugation method[31]. The hydrodynamic size of dispersed particles and their effective densities allows to estimate the fraction of administered dose (fD) that would deposit on cells as a function of time (Figure 4). After 24 hours of incubation in both SMI-100 and MEM medium, approximately 30% to 40% of the administered SiO_2 NPs would be delivered to the cells. Although 100% of the Ag NPs would be delivered to the cells in SMI-100 media after 24 hours of incubation, deposition is slower in MEM medium, resulting to only 50% deposition in 24 hours. This information is used to ensure standardized amount of delivered dose of NPs between different culture formats and media utilized in the study.

3.4 Effect of NPs on barrier integrity of 3D EpiIntestinal™ tissue

The capacity of NPs to induce permeabilization to 3D EpiIntestinal™ tissue was assessed by measuring both FITC-dextran paracellular transport (Figure 5A) and TEER (Figure 5B). Incubation of the tissue in the presence of 50 µg/ml FITC-dextran in the apical chamber did not cause any increase in FITC-dextran paracellular transport nor any decrease in TEER values. These results confirm that under the existing experiment conditions, the tested NPs did not affect the permeabilization of 3D EpiIntestinal™ tissue. The tissue barrier remained intact following SiO_2 and Ag NPs exposure. Cytochalasin B (Cyto B) at 20 µg/ml was used as positive control to ensure validity of both assays. Addition of Cyto B caused a significant increase in FITC-dextran paracellular transport (25%, $p < 0.05$) and a significant decrease in TEER value (68%, $p < 0.05$).

3.5 Genotoxicity assessment of NPs in *in vitro* 3D EpiIntestinal™ tissue

The genotoxic potential of the tested NPs in 3D EpiIntestinal™ tissue was investigated through the newly developed reconstructed micronuclei cytome (RICyt) assay protocol[33]. Micronuclei (Figure 6) alongside with other cell types and nuclei anomalies (Table 1) were scored for genotoxicity assessment. Neither genotoxicity nor cytotoxicity were detected in tissues exposed with SiO_2 NP (Figure 6A) and Ag NP (Figure 6B). Other than micronuclei, the tested NPs also did not induce other forms of nuclear anomalies as depicted in Table 1. Solvent controls, 10% H_20 and 5% citrate buffer, produced low level of basal micronuclei frequency (~1.2-1.5%). The positive control, mitomycin C at 1 µg/ml, consistently produced ~2.2-fold increase ($p < 0.05$) in micronuclei production and 8.12% increase ($p < 0.05$) in karyorrhexis (i.e., apoptosis).

The NPs were also tested using the reconstructed intestine comet (RICom) assay protocol. For both NPs two tailed one-way ANOVA showed no statistically significant difference

between groups for % tail DNA and no values were above the upper historical negative control range (5.16%), with minimal accompanying cytotoxicity. A clear negative result (Figure 7, Table 2) was shown. The positive control, ethyl methanesulfonate at 500 µg/ml, consistently produced a significant difference in % tail DNA ($p < 0.05$).

Table 1. Comet genotoxicity assessment of NPs in 3D EpiIntestinal™ tissue. Tissues were exposed to test articles for 2 days via apical treatment. At the end of treatment, tissues were dissociated to single cells for comet slide preparation. One hundred viable comets were scored per microtissue to determine the median % tail DNA. The mean % tail DNA from three independent experiments are shown. +ve control; 500 µg/ml ethyl methanesulfonate. * $p < 0.01$ in two tailed one-way ANOVA with Tukey's post-hoc test, relative to other sample groups in the corresponding series.

Test Material	Test concentration (µg/ml)	Tail DNA %		Relative Cell Count %	
		Mean	STDEV	Mean	STDEV
SiO_2 NP	solvent	2.46	0.65	100.00	0.00
	25.0	3.22	0.68	98.30	0.30
	50.0	2.29	0.59	96.71	9.46
	100.0	2.28	0.23	82.56	10.38
	+ve control	29.17 *	2.96	93.96	44.41
Ag NP	solvent	1.85	0.49	100.00	0.00
	25.0	2.69	0.44	83.00	7.94
	50.0	2.18	0.80	90.65	11.37
	100.0	3.11	0.47	83.76	21.11
	+ve control	30.89 *	2.45	86.10	14.38

SiO_2 NP: silicon dioxide nanoparticles; AgNP: silver nanoparticles.

Table 2. Frequencies of cell types and nuclear anomalies in scored in 3D EpiIntestinal™ tissue. Nanoparticles were applied to the apical surface of 3D EpiIntestinal™ tissues for 10 days.

Tissues were dissociated into single cell suspensions and fixed in Carnoy's fixative. One thousand total cells were scored per microtissue to determine the frequency of MN and cytome induction. The results from three independent experiments are shown. Each experiment consisted of a single microtissue per test dose. Mitomycin C (1 μg/ml) were used as positive control. Water (10%) and citrate buffer (5%) were solvent controls. Data are reported as percentage (mean ± SD). *$p < 0.05$; **$p < 0.001$ compared with other MN % sample groups in the corresponding series.

SiO_2 NP (µg/ml)	MN	Buds	Mono	BN	CC	KR	PY	KL
10% H2O	1.47 ± 0.03	0.40 ± 0.10	92.10 ± 1.36	0.87 ± 0.24	0.20 ± 0.12	3.87 ± 0.71	0.40 ± 0.25	0.70 ± 0.06
1	1.50 ± 0.12	0.30 ± 0.15	93.57 ± 1.32	0.73 ± 0.32	0.10 ± 0.10	3.00 ± 0.70	0.40 ± 0.12	0.40 ± 0.25
10	1.90 ± 0.06	0.57 ± 0.09	90.9 ± 0.76	1.13 ± 0.20	0.13 ± 0.07	3.80 ± 0.35	0.77 ± 0.33	0.80 ± 0.15
50	1.76 ± 0.14	0.60 ± 0.15	90.31 ± 2.01	0.93 ± 0.33	0.23 ± 0.19	4.60 ± 0.97	0.53 ± 0.27	1.03 ± 0.49
MMC 1 µg/ml	3.13 ± 0.26**	0.93 ± 0.07	85.17 ± 1.28	1.33 ± 0.12	0.13 ± 0.09	8.40 ± 1.33	0.53 ± 0.33	0.37 ± 0.07

AgNP (µg/ml)	MN	Buds	Mono	BN	CC	KR	PY	KL
Citrate buffer	1.63 ± 0.19	0.57 ± 0.19	92.77 ± 1.05	1.07 ± 0.38	0.07 ± 0.03	3.07 ± 0.22	0.67 ± 0.33	0.17 ± 0.09
1	1.87 ± 0.32	0.47 ± 0.18	92.73 ± 0.73	0.97 ± 0.15	0.07 ± 0.07	2.77 ± 0.27	0.57 ± 0.09	0.57 ± 0.13
10	1.77 ± 0.32	0.27 ± 0.07	94.14 ± 1.00	1.07 ± 0.19	0.03 ± 0.03	1.93 ± 0.41	0.47 ± 0.29	0.33 ± 0.23
50	1.57 ± 0.27	0.33 ± 0.15	93.93 ± 0.86	1.10 ± 0.21	0.07 ± 0.07	2.43 ± 0.79	0.33 ± 0.03	0.23 ± 0.03
MMC 1 µg/ml	3.13 ± 0.26*	0.93 ± 0.07	85.17 ± 1.28	1.33 ± 0.12	0.13 ± 0.09	8.40 ± 1.33	0.53 ± 0.33	0.37 ± 0.07

MN, micronuclei; Buds, nuclear buds; Mono, mononucleated cells (basal and differentiated); BN, binucleated cells; CC, condensed chromatin; KR, karyorrhexis; PY, pyknosis; KL, karyolysis

3.6 Genotoxicity assessment of NPs in *in vitro* 2D Caco-2 cells

The selected nanomaterials were assessed for genotoxicity in Caco-2 colon cell line with the cytokinesis-blocked micronucleus assay protocol according to OECD TG487 guidelines. Both NPs did not induce significant micronuclei numbers and cytotoxicity compared to the solvent control (Figure 8, Table 3). For the samples tested with Ag NPs standard (NanoComposix, Ag75, AGCO75), Caco-2 showed significant dose dependent cytotoxicity ($p < 0.0001$) compared with the solvent control. However, there were no significant genotoxicity detected across the treatment groups.

Table 3. Frequency of micronucleus scored in Caco-2 cells treated with A. SiO_2 NP and B. Ag NP. The results from three independent experiments are shown. Mitomycin C (0.03 µg/ml) were used as positive control. Water (10%) and citrate buffer (10%) were solvent controls. The values are expressed as percentages compared to solvent controls and presented as mean ± SD.

A. SiO_2NP, E551 (µg/ml)	**% MN**	**% Cell Viability**
10% H_2O	2.99 ± 0.49	100 ± 0.00
1	2.89 ± 0.94	96.78 ± 0.98
10	3.26 ± 0.53	98.63 ± 6.96
50	3.49 ± 0.83	98.33 ± 8.48
MMC (µg/ml)	**% MN**	**% Cell Viability**
0.03	10.68 ± 0.41	85.61 ± 10.28

B. AgNP, AGC075 (µg/ml)	% MN	% Cell Viability
10% Citrate Buffer	3.66 ± 1.11	100 ± 0.00
1	5.13 ± 2.43	86.17 ± 6.35
2	5.65 ± 1.93	55.69 ± 3.21
MMC (µg/ml)	**% MN**	**% Cell Viability**
0.03	13.14 ± 4.15	82.15 ± 1.88

3.7 Hyperspectral imaging (HSI) and spectral mapping of NPs-exposed 3D EpiIntestinal™ tissue

Hyperspectral imaging was performed to examine SiO_2 and Ag NP penetration in 3D EpiIntestinal™ tissue. Prior to HSI acquisition of tissues, individual spectral libraries (SL) were obtained for pristine SiO_2 and Ag NPs (supplementary Figure 1A and 1B). Reference spectra collected from SiO_2 NPs had consistent profiles over 450 – 800 nm. In contrast, the spectra collected from Ag NPs showed more varied profiles over the similar range of wavelengths. Next, brightfield and darkfield images were obtained for controls and NPs treated 3D tissues, followed by spectral mapping using the Cytoviva™ ENVI software to identify internalized NPs. Tissue imaging in Citrate buffer (CB) group was included as a control because Ag NPs were suspended in CB.

After 48hours of exposure to 50 µg/ml of SiO_2 NPs, SAM images revealed localized spectral profiles of SiO_2 NPs mainly accumulated at the bottom of the tissue, which was not observed

in the controls (Figure 9). Spectral profile of Ag NPs was less intense but evenly distributed throughout the tissue sample (Figure 9).

3.8 Intracellular localization of NPs in 3D EpiIntestinal™ tissue and 2D Caco-2 gut cell line

To study the internalization, localization and cellular impact of the test NPs on 3D intestinal tissue, TEM was performed. The TEM micrographs indicated internalization of SiO_2 and Ag NPs in both 3D EpiIntestinal™ tissue as well as 2D Caco-2 cells, Figure 10 and Figure 11, respectively. The untreated control (CTR) tissue appeared healthy as evidenced by 1) healthy nuclear morphology with intact nuclear membrane 2) presence of brush border-like morphology, and 3) presence of gap junctions (Figure 10 top panel). Tissues exposed to SiO_2 NPs displayed cytosolic localization of NPs and extensive cytoplasmic vacuolization. Additionally, there was an increase in the number of perinuclear autophagosomes, although no change in nuclear morphology was observed. Like SiO_2, Ag NPs also showed cytosolic localization, however, the nucleus appeared fragmented with increased appearance of micronuclei and autophagosomes around the nucleus. Similar observations were made in 2D cells (Figure 11) where SiO_2 caused formation of large cytoplasmic vacuoles. Although Ag NPs uptake was much lower compared to SiO_2, the cellular damages observed were more significant. Furthermore, elemental mapping performed with Scanning-TEM (STEM) in Figure 12, showed the presence of Si and Ag, as depicted by the red channels, inside the cells, confirming the corresponding uptake of NPs by the cells.

4.0 Discussion

This study compared two in vitro models—2D Caco-2 cells and 3D EpiIntestinal™—to evaluate the impact of food-based NPs: SiO_2 (E551) and Ag (AGCO75) on cellular responses and

genotoxicity in the human gastrointestinal system. The 2D Caco-2 model is appreciated for its simplicity, cost-effectiveness, and ease of use but lacks the physiological complexity and tissue architecture of in vivo conditions. Caco-2 cells are also susceptible to oxidant induced effects and are not necessarily a good model system to investigate toxicity in the gut[38,39]. In contrast, the 3D EpiIntestinal™ model offers a more physiologically relevant context, replicating in vivo tissue structure and cell interactions. it has also been shown that general metabolic capacity is greater in the EpiIntestinal™ model, which more closely resembles metabolic capacity in the gut[39]. Hence, we sought to determine if the EpiIntestinal™ model is a suitable platform for evaluating the toxicity of ingested food-based NPs, particularly in the context of genotoxicity, using adapted test protocols.

Before delving into cellular responses, it is crucial to address various factors influencing the behavior of NPs in physiological environment. These factors include chemical composition, size, shape, charge, surface area and hydrophobicity. The physicochemical and colloidal properties of NPs play a pivotal role in governing their nano-bio interactions with cells and surrounding tissues. Therefore, it is imperative to have well-characterized and stable colloidal NPs to ensure reproducibility in nanotoxicological studies. To attain this, a comprehensive characterization of these factors was performed. Additionally, an integrated method, previously developed by DeLoid et al., was also employed in this study. This method involves dispersing the NPs, characterizing their colloidal stability, and estimating the delivered dose for subsequent in vitro studies[31]. Through the application of this model, respective delivered dosage of a stable NPs dispersion was exposed to the 3D tissue and Caco-2 cell line.

Upon exposure of NPs to the intestinal tissue, the tissue's barrier integrity was examined to investigate the interaction between NPs and biological barriers of the tissue. We evaluated the capacity of NPs to induce permeabilization by measuring both FITC-dextran paracellular

transport and TEER. Interestingly, incubation of the tissue with NPs, specifically at a concentration of 50 µg/ml, did not result in any significant increase in FITC-dextran paracellular transport or decrease in TEER values. The intactness of the tissue barrier following exposure to NPs suggest that under the tested conditions, both NPs did not disrupt the integrity of 3D EpiIntestinal™ tissue barrier. This is particularly significant in the context of NP toxicity assessment, as disruptions in epithelial barriers could lead to increased absorption of NPs and potentially adverse effects. To validate the reliability of the assays used in this study, Cytochalasin B (Cyto B), a known disruptor of the cytoskeleton and inducer of permeabilization, was employed as a positive control. As expected, addition of Cyto B resulted in a significant increase in FITC-dextran paracellular transport and a substantial decrease in TEER value, confirming the sensitivity and validity of both assays.

Next, we investigated the cytotoxicity and genotoxicity induced by these NPs in 3D intestinal tissue and Caco-2 cell line. The findings from micronuclei cytome (RICyt) assay indicated that neither SiO_2 nor Ag NPs induce genotoxicity nor cytotoxicity in dosed 3D EpiIntestinal™ tissue. This observation was further supported by the absence of other nuclear anomalies apart from micronuclei. Additionally, the solvent controls produced only a low level of basal micronuclei frequency, confirming the validity of the assay. The positive control, mitomycin C, demonstrated the assay's sensitivity by inducing a significant increase in micronuclei production and karyorrhexis. Furthermore, the reconstructed intestine comet (RICom) assay protocol also yielded negative results for both SiO_2 and Ag NPs, with no statistically significant increase in % tail DNA observed above historical negative control range, and minimal accompanying cytotoxicity. The genotoxicity findings in the 3D EpiIntestinal™ platform is reproducible in OECD recommended cell line, Caco-2, and in line with published literature. Consistent with the findings in the 3D EpiIntestinal™ tissue model, neither SiO_2 NPs nor Ag

NPs induced significant micronuclei formation or cytotoxicity compared to the solvent control in the 2D Caco-2 cultures. However, it is important to note that the Ag NPs standard exhibited significant dose-dependent cytotoxicity in Caco-2 cells, although no significant genotoxicity was detected across the treatment groups. This could be explained by the intactness of the 3D intestinal tissue barrier upon exposure of the Ag NPs, compared to 2D cultures. This barrier effect may be providing a protective effect, limiting exposure of cells to exogenous generation of ROS[39]. Overall, the results from both the 3D EpiIntestinal™ tissue model and the 2D Caco-2 colon cell line suggest that the tested NPs, SiO_2 and Ag, do not present genotoxic and intestinal barrier dysfunction risks to the human gut under the tested conditions, although a dose-dependent Ag NP induced reduction in cell viability was observed in Caco-2 cells.

In addition to assessing genotoxicity, HSI and TEM were employed to investigate the potential of SiO_2 and Ag NPs to penetrate the tissue layers and cellular uptake. These complementary techniques provide valuable insights into the interactions between NPs and biological tissues, shedding light on their distribution and localization within cellular compartments. By examining the spatial distribution of NPs within the tissue layers and characterizing their cellular uptake, we can further elucidate the mechanisms underlying the biological effects observed in our genotoxicity assessments. Both SiO_2 and Ag NPs were internalized by the 3D EpiIntestinal™ tissues and localized in the cytosolic region. HSI showed localized spectral profiles of SiO_2 NPs at the bottom of the tissue, whereas even distribution of Ag NPs throughout the tissue indicates differential penetration behaviors between the two NPs within the 3D intestinal tissue. Though internalized, both NPs produce no damaging effects to the barrier of intestinal epithelium, as discussed earlier, suggesting that tight junction proteins are not targeted for their entry into the cells. Further investigation into the intracellular localization and impact of NPs was conducted using TEM. Both SiO_2 and Ag NPs

were found to be internalized by the cells in 3D tissue as well as in 2D cell models. The tissues exposed to SiO_2 NPs displayed cytosolic vacuolization and an increase in perinuclear autophagosomes. Similarly, Ag NPs exhibited cytosolic localization, yet induced nuclear fragmentation, micronuclei formation, and increased autophagosome, suggesting more pronounced cellular damage compared to SiO_2 NPs. This phenomenon could be due to the oversaturation or off-target effect from high dose of both NPs (50 µg/ml) added to the tissues. The presence of autophagosomes infers potential autophagic processing of NPs and could be essential for maintenance of intestinal epithelial cell integrity and subsequent lysosomal exocytosis of the NPs[40]. In comparison, Caco-2 cells treated with SiO_2 NPs exhibited the formation of large cytoplasmic vacuoles, while Ag NPs induced lower cell uptake but more significant cellular damage. Elemental mapping with scanning-TEM (STEM) confirmed the presence of Si and Ag elements inside the cells, further validating NP uptake.

Earlier, there have been several studies carried out to investigate possible genotoxic effects of SiO_2 and Ag NPs. Negative findings were observed in in vitro studies evaluating SiO_2 NPs induced DNA fragmentation in comet assay[41], chromosomal aberrations, and micronuclei[42]. In vivo studies also showed negative findings in comet assay in duodenum and colon in rats, following oral route of exposure[43], in agreement with a separate study that indicated SiO_2 NPs had a low potential to cross the gastrointestinal tract[44]. Overall, SiO_2 NPs used as a food additive did not raise concerns with respect to genotoxicity[45]. In animal studies with oral acute exposure in adult mice, Ag NPs were mostly accumulated in duodenum. Localization analysis showed that Ag NPs scatter in cytoplasm or membrane bound organelles but never in the nucleus, accounting for the lack of genotoxicity evaluated by comet or micronucleus assay[46]. It was concluded that the use of the Ag NPs as an additive at up to 0.025% w/w in food contact

material does not raise safety concerns for the consumer[47]. The genotoxicity data in 2D and 3D models from our study are in line with and supported by these published findings.

5.0 Conclusion

The integration of 3D intestinal tissue models and 2D Caco-2 gut cell line models provides a comprehensive approach to understanding the behavior of food-based NPs. By combining these models, we can overcome limitations and gain a nuanced perspective on NP interactions. This approach is crucial for accurately predicting NP toxicity in the food industry. Utilizing complementary 2D and 3D assays allows for initial genotoxicity assessment in 2D models, followed by validation in 3D models simulating relevant exposure routes, such as the intestinal route. In this study, by using both 2D Caco-2 cell cultures and 3D EpiIntestinal™ small intestinal microtissues, we found that neither genotoxicity nor cytotoxicity were detected in the 3D tissues after SiO_2 and Ag NP treatment, while the 2D cultures exhibited cytotoxic response from Ag NP treatment. Both NPs were internalized into cells in both 2D and 3D culture models. Overall, the 3D small intestinal tissue model was found to be more resilient to NP treatment compared to 2D Caco-2 cell monolayers. Moving forward, the development and validation of 3D models will enhance predictive capabilities and improve prioritization of animal testing based on exposure risk. While the EpiIntestinal™ microtissues system shows promise as an initial testing platform, further validation is needed for accurate toxicity prediction. Continued research in this area will advance our understanding of NP interactions in gastrointestinal contexts, leading to safer food-based nanoparticle products and enhanced consumer safety.

6.0 Acknowledgment

This research was supported by the Industry Alignment Fund (Pre-Positioning; IAF-PP-H18/01/a0/G14), Biomedical Research Council (BMRC, A*STAR). The authors acknowledge the Facility for Analysis, Characterization, Testing and Simulation (FACTS), NTU, for the support in electron microscopy analysis.

7.0 References

1. Organization, W. H. Food additives. Preprint at (2022).
2. Ashfaq, A., Khursheed, N., Fatima, S., Anjum, Z. & Younis, K. Application of nanotechnology in food packaging: Pros and Cons. *J Agric Food Res* **7**, 100270 (2022).
3. Onyeaka, H., Passaretti, P., Miri, T. & Al-Sharify, Z. T. The safety of nanomaterials in food production and packaging. *Curr Res Food Sci* **5**, 763–774 (2022).
4. Vance, M. E. *et al.* Nanotechnology in the real world: Redeveloping the nanomaterial consumer products inventory. *Beilstein J Nanotechnol.* **6**, 1769–1780 (2015).
5. Cao, Y. *et al.* Consideration of interaction between nanoparticles and food components for the safety assessment of nanoparticles following oral exposure: A review. *Environ Toxicol Pharmacol.* **46**, 206–210 (2016).
6. Dekkers, S. *et al.* Presence and risks of nanosilica in food products. *Nanotoxicology* **5**, 393–405 (2011).
7. Wang, H., Du, L. J., Song, Z. M. & Chen, X. X. Progress in the characterization and safety evaluation of engineered inorganic nanomaterials in food. *Nanomedicine (Lond).* **8**, 2007–2025 (2013).
8. Barahona, F., Ojea-Jimenez, I., Geiss, O., Gilliland, D. & Barrero-Moreno, J. Multimethod approach for the detection and characterisation of food-grade synthetic amorphous silica nanoparticles. *J Chromatogr A* **1432**, 92–100 (2016).
9. Athinarayanan, J., Periasamy, V. S., Alsaif, M. A., Al-Warthan, A. A. & Alshatwi, A. A. Presence of nanosilica (E551) in commercial food products: TNF-mediated oxidative stress and altered cell cycle progression in human lung fibroblast cells. *Cell Biol Toxicol* **30**, 89–100 (2014).
10. Yoo, N.-K., Jeon, Y.-R. & Choi, S.-J. Determination of two differently manufactured silicon dioxide nanoparticles by cloud point extraction approach in intestinal cells, intestinal barriers and tissues. *Int J Mol Sci* **22**, 7035 (2021).
11. Peters, R. *et al.* Presence of nano-sized silica during in vitro digestion of foods containing silica as a food additive. *ACS Nano* **6**, 2441–2451 (2012).
12. Sukhanova, A. *et al.* Dependence of nanoparticle toxicity on their physical and chemical properties. *Nanoscale Res Lett* **13**, 1–21 (2018).
13. Lamas, B., Martins Breyner, N. & Houdeau, E. Impacts of foodborne inorganic nanoparticles on the gut microbiota-immune axis: potential consequences for host health. *Part Fibre Toxicol* **17**, 1–22 (2020).

14. Murugadoss, S. *et al.* Toxicology of silica nanoparticles: an update. *Arch Toxicol* **91**, 2967–3010 (2017).
15. Napierska, D., Thomassen, L. C., Lison, D., Martens, J. A. & Hoet, P. H. The nanosilica hazard: another variable entity. *Part Fibre Toxicol* **7**, 1–32 (2010).
16. Gaillet, S. & Rouanet, J.-M. Silver nanoparticles: their potential toxic effects after oral exposure and underlying mechanisms--a review. *Food and Chemical Toxicology.* **77**, 58–63 (2015).
17. Istiqola, A. & Syafiuddin, A. A review of silver nanoparticles in food packaging technologies: Regulation, methods, properties, migration, and future challenges. *Journal of the Chinese Chemical Society.* **67**, 1942–1956 (2020).
18. McClements, D. J. & Xiao, H. Is nano safe in foods? Establishing the factors impacting the gastrointestinal fate and toxicity of organic and inorganic food-grade nanoparticles. *NPJ Sci Food* **1**, 6 (2017).
19. Jaswal, T. & Gupta, J. A review on the toxicity of silver nanoparticles on human health. *Mater Today Proc* **81**, 859–863 (2023).
20. Yazdimamaghani, M., Moos, P. J., Dobrovolskaia, M. A. & Ghandehari, H. Genotoxicity of amorphous silica nanoparticles: Status and prospects. *Nanomedicine* **16**, 106–125 (2019).
21. Lee, J., Lilly, G. D., Doty, R. C., Podsiadlo, P. & Kotov, N. A. In vitro toxicity testing of nanoparticles in 3D cell culture. *Small.* **5**, 1213–1221 (2009).
22. Lee, J., Cuddihy, M. J. & Kotov, N. A. Three-dimensional cell culture matrices: state of the art. *Tissue Eng Part B Rev.* **14**, 61–86 (2008).
23. Griffith, L. G. & Swartz, M. A. Capturing complex 3D tissue physiology in vitro. *Nat Rev Mol Cell Biol.* **7**, 211–224 (2006).
24. Helander, H. F. & Fändriks, L. Surface area of the digestive tract - revisited. *Scand J Gastroenterol.* **49**, 681–689 (2014).
25. Egger, L. & others. The harmonized INFOGEST in vitro digestion method: From knowledge to action. *Food Research International* **88**, 217–225 (2016).
26. Temple, J., Velliou, E., Shehata, M. & Lévy, R. Current strategies with implementation of three-dimensional cell culture: the challenge of quantification. *Interface Focus* **12**, (2022).
27. Ahmad, M. K., Khan, A. A., Ali, S. N. & Mahmood, R. Chemoprotective Effect of Taurine on Potassium Bromate-Induced DNA Damage, DNA-Protein Cross-Linking and Oxidative Stress in Rat Intestine. *PLoS One* **10**, e0119137 (2015).
28. Ayehunie, S. *et al.* Human Primary Cell-Based Organotypic Microtissues for Modeling Small Intestinal Drug Absorption. *Pharm Res.* **35**, 72 (2018).
29. Hinderliter, P. M. *et al.* ISDD: A computational model of particle sedimentation, diffusion and target cell dosimetry for in vitro toxicity studies. *Part Fibre Toxicol.* **7**, 36 (2010).
30. Rakshit, M. *et al.* Hydroxyapatite Particles Induced Modulation of Collagen Expression and Secretion in Primary Human Dermal Fibroblasts. *Int J Nanomedicine.* **15**, 4943–4956 (2020).
31. DeLoid, G. *et al.* Estimating the effective density of engineered nanomaterials for in vitro dosimetry. *Nat Commun* **5**, 3514 (2014).
32. Ayehunie, S. *et al.* Novel 3D Human Small Intestinal Tissue Model (EpiIntestinal TM) to Assess Drug Permeation & Inflammation. (2014).

33. Lim, H. K. *et al. Development of Reconstructed Intestinal Micronucleus Cytome (RICyt) Assay in 3D Human Gut Model for Genotoxicity Assessment of Orally Ingested Substances*. (Arch Toxicol, 2022).
34. Tolbert, P. E., Shy, C. M. & Allen, J. W. Micronuclei and other nuclear anomalies in buccal smears: methods development. *Mutat Res.* **271**, 69–77 (1992).
35. Thomas, P. *et al.* Buccal micronucleus cytome assay. *Nat Protoc.* **4**, 825–837 (2009).
36. Hughes, C. O., Lim, H. K., Tan, J. C. W., Leavesley, D. I. & Smith, B. P. C. Reconstructed human intestinal comet assay, a possible alternative in vitro model for genotoxicity assessment. *Mutagenesis* **38**, 139–150 (2023).
37. Cohen, J. M., Beltran-Huarac, J., Pyrgiotakis, G. & Demokritou, P. Effective delivery of sonication energy to fast settling and agglomerating nanomaterial suspensions for cellular studies: Implications for stability, particle kinetics, dosimetry and toxicity. *NanoImpact* **10**, 81–86 (2018).
38. Baker, S. S. & Baker, R. D. Caco-2 cell metabolism of oxygen-derived radicals. *Dig Dis Sci* **38**, 2273–2280 (1993).
39. Markus, J. *et al.* Human small intestinal organotypic culture model for drug permeation, inflammation, and toxicity assays. *In Vitro Cell Dev Biol Anim* **57**, 160–173 (2021).
40. Sipos, A. *et al.* Alveolar epithelial cell processing of nanoparticles activates autophagy and lysosomal exocytosis. Am J Physiol Lung Cell Mol Physiol.
41. Gonzalez, L. *et al.* Exploring the aneugenic and clastogenic potential in the nanosize range: A549 human lung carcinoma cells and amorphous monodisperse silica nanoparticles as models. *Nanotoxicology* **4**, 382–395 (2010).
42. Vecchio, G., Fenech, M., Pompa, P. P. & Voelcker, N. H. Lab-on-a-chip-based high-throughput screening of the genotoxicity of engineered nanomaterials. *Small.* **10**, 2721–2734 (2014).
43. Tarantini, A. *et al.* Genotoxicity of synthetic amorphous silica nanoparticles in rats following short-term exposure. Part 1: oral route. *Environ Mol Mutagen.* **56**, 218–227 (2015).
44. Yang, Y. X. *et al.* Evaluation of the toxicity of food additive silica nanoparticles on gastrointestinal cells. *J Appl Toxicol.* **34**, 424–435 (2014).
45. oFAaNSat, F. Ep. *et al.* Re-evaluation of silicon dioxide (E 551) as a food additive. *EFSA Journal.* **16**, e05088 (2018).
46. Narciso, L. *et al.* Genotoxicity, biodistribution and toxic effects of silver nanoparticles after in vivo acute oral administration. *NanoImpact* **18**, 100221 (2020).
47. Panel, E. on Food Contact Materials EaPA, Lambré C, Barat Baviera JM, Bolognesi C, Chesson A, Cocconcelli PS, et al. Safety assessment of the substance silver nanoparticles for use in food contact materials. *EFSA Journal.* **19**, e06790 (2021).

Assessing nanotoxicity of food-relevant particles: A comparative analysis of cellular responses in cell monolayers versus 3D gut epithelial cultures

Archana Gautam[1 #], Hui Kheng Lim[2,3,4 #], Jasmine Jia'En Li[5 #], Christopher Owen Hughes[2,3,4], Calvin Wee Sing Yeo[5], Moumita Rakshit[1], David Ian Leavesley[3], Michelle Jing Sin Lim[4,6], Joseph Choon Wee Tan[4], Li Yi Tan[1], Joanne Sheot Harn Chan[5], Benjamin Paul Chapman Smith[2,4,6,7 *], Kee Woei Ng[1,3,8 **]

[1]School of Materials Science and Engineering, Nanyang Technological University, 50 Nanyang Avenue, Singapore

[2]Innovations in Food and Chemical Safety (IFCS) Programme, Agency for Science, Technology and Research, Singapore

[3]Skin Research Institute of Singapore (SRIS), Agency for Science, Technology and Research, Singapore

[4]Future Ready Food Safety Hub (a joint initiative of A*STAR, SFA & NTU), Nanyang Technological University, Singapore

[5]National Centre for Food Science, Singapore Food Agency, Singapore

[6]Singapore Institute of Food and Biotechnology Innovation (SIFBI), Agency for Science, Technology and Research, Singapore

[7]Chemical Senses Center, 3500 Market Street, Pennsylvania, 19104, USA

[8]Nanyang Environment and Water Research Institute, Nanyang Technological University, 1 Cleantech Loop, CleanTech One, Singapore

[#] These authors contributed equally to this work

Corresponding authors:

*bsmith@monell.org

**kwng@ntu.edu.sg

Abstract

Engineered nanoparticles (NPs) are extensively used in the food industry, yet safety concerns remain. The lack of validated methodologies is a bottleneck towards resolving this uncertainty. Hence, the current study aims to compare two cell models by examining the toxicological impacts of two food-relevant NPs (SiO_2 and Ag) on intestinal epithelia using monolayer Caco-2 cells and full-thickness 3D tissue models of human small intestines (EpiIntestinal™). Comprehensive characterization and dosimetric analysis of the NPs were performed to determine effective doses and model realistic exposures. Neither genotoxicity nor cytotoxicity were detected in the 3D tissues after NP treatment, while the 2D cultures exhibited cytotoxic response from Ag NP treatment for 24 hr at 1 μg/ml. Hyperspectral imaging and transmission electron microscopy confirmed uptake of both NPs by cells in both 2D and 3D culture models. Ag NPs caused an increase in autophagy, whereas SiO_2 NPs induced increased cytoplasmic vacuolization. Based on realistic exposure levels studied, the 3D small intestinal tissue model was found to be more resilient to NP treatment compared to 2D cell monolayers. This comparative approach towards toxicological assessment of food relevant NPs could be used as a framework for future analysis of NP behavior and nanotoxicity in the gut.

Keywords: Nanoparticles, nanotoxicology, intestine, genotoxicity, 3D models

1.0 Introduction

The rapid advancement in nanotechnology, in the recent years, have paved the way for the development of innovative nanomaterials, particularly within the realm of food science. Today, the majority of our food products are enriched with various food-based additives intentionally incorporated to extend their shelf-life, enhance safety, freshness, taste, texture and appearance, as highlighted by the World Health Organization[1]. Significantly, researchers have revealed that a substantial portion of these approved food additives exists in nano-sized forms, underscoring the pervasive integration of engineered nanomaterials in the food industry. These nanomaterials play a pivotal role in elevating the overall food quality, flavor, shelf life, aesthetics, and nutritional value of food products. Furthermore, they have become indispensable in the development of next-generation food contact materials. Their unique physio-chemical properties contribute to improved barrier properties in food packaging and they serve as sensors for food quality and freshness indicators[2]. However, the widespread incorporation of nanomaterials into foods and food contact materials has prompted concerns regarding their potential impact on human health[3].

Consumers are exposed to NPs through ingestion of NPs-containing food products or beverages, ingestion being the third route of exposure, after dermal and inhalation[4,5]. Silicon Dioxide (SiO_2) NPs are among the most widely used NPs and a registered food additive E551 in the European Union. They are used as an anti-caking agent[6,7] in powdered or granulated materials to prevent clumping, and as a carrier, thickener, and color diluent in products such as confectionaries, powdered mixtures, and seasonings[8]. Reports show the presence of silica NPs in food products with a diameter between 10 and 50 nm[9]. Additionally, their size could be further reduced during the digestion process and modification of their aggregation state on contact with the biological fluids[10]. Silica NPs in food prepared with E551 additive was

reported to be present after intestinal digestion suggesting that upon consumption of foods containing E551, the gut epithelium is most likely exposed to nano-size silica[11]. Previous research highlights that these NPs possess the ability to easily penetrate the cell membranes, interacting with human cells and tissues, raising potential health risks given their inherent characteristics[12]. Likewise, the literature contains a wealth of studies examining the intestinal toxicity of silica NPs, including those found in the E551 additive where they have been reported to cause injuries to cells, tissues, and organs in vitro and in vivo[13–15].

Silver (Ag) NPs are known to possess antimicrobial and antioxidant properties and they have been used as antimicrobial agents in foods and food packaging materials[16]. While they can inhibit biofilm formation and browning in fresh cut fruits it is possible that some of these NPs may migrate from these packaging materials into the foods so that they could be ingested by humans. The addition of Ag NPs into food packaging can also improve their barrier and mechanical properties[17]. At present, there is still limited information on the potential toxicity of Ag NPs ingested with foods, with some studies reporting no toxicity and others reporting appreciable toxicity in humans[16]. Numerous animal studies have reported that dietary intake of Ag NPs caused lymphocyte infiltration, pigmentation of villi, discharge of mucus granules and abnormal mucus composition in the intestine. Animal studies have further reported that these NPs can accumulate in various organs after ingestion, including the liver, kidneys, spleen, stomach, and small intestine[18]. However, it is not clear whether these NPs have toxic effects when consumed by humans in the levels which are close to those actually achievable through food consumption. Specific to genotoxic effects of both SiO_2 and Ag NPs, contradictory reports are found in the literature [19,20]. Comparing across the literature presents significant challenges primary because of non-harmonized methodologies.

Nevertheless, these studies are fraught with significant limitations. Typically, the NPs were incubated with intestinal cell lines, predominantly Caco-2, without accounting for the presence of an epithelial barrier in the real tissue, and the mucus layer. This barrier serves as the first line of defense against invasion of foreign microorganisms, including NPs. Hence, based on the facts reported in these studies, synthetic food additives in the food industry needs to be reexamined in a more realistic model, along with their physiochemical properties fully characterized so that the safety level for human intake can be entirely revealed. Therefore, to overcome these drawbacks, our study takes a pioneering approach, addressing these limitations through the implementation of a 3D intestinal epithelial model for a more comprehensive evaluation of toxicity. This study focuses on investigating the impact of two extensively utilized food-grade NPs, SiO_2 (E551) and Ag (AGCO75), using both traditional 2D cell cultures and advanced 3D intestinal epithelial models. Our comprehensive evaluation encompasses their characteristics, solubility, cytotoxicity, cellular uptake and localization, as well as genotoxicity. By delving into these aspects, we aim to provide valuable insights into the potential risks associated with these commonly employed food-based NPs, contributing to the ongoing discourse on their responsible use in the food industry.

Effectively all cells in the body are organized and resided in a well-organized 3D environment with extensive cell-cell and cell-matrix interactions, which is essential for their growth and metabolism[21]. 2D cell cultures do not adequately recapitulate the appropriate level of in vivo cellular responses because cell–cell and cell–matrix interactions are markedly reduced in the monolayer cell culture raised on a flat culture dish[22]. Though providing valuable information, tests performed with 2D monolayer cultures do not always accurately predict actual toxicity of in vivo conditions due to the absence of key biological and physiological processes[23]. The gut makes up a large portion of the body's external surface[24] and the small intestine is where

around 90% of the digestion and absorption of food occurs[25]. Thus, it is a major exposure site of ingested toxicants. Whilst 3D models can lack consistency due to variabilities across multiple factors[26] , the production of EpiIntestinal™ microtissues are highly standardized and validated as a representative in vitro mimicry system with structural, biochemical, physiological, functional, and mechanistic properties highly resembling the human gut[27]. When use in food hazard identification, this model offers site-of-first contact information of ingested material. Unlike spheroids or organoids which have issues with NPs penetration, the upward facing luminal structure (apical side) of EpiIntestinal™ microtissues allows homogenous exposure to NPs. It is worth noting that loss of tissue barrier integrity is the first indication of any dysfunction or damage to intestinal epithelium. Assessment of barrier function is permissible due to the accessibility to intestinal luminal surfaces. EpiIntestinal™ microtissues can be cultured for an extended period of time up to 28 days[28], which allows multiple dosing and long-term studies. Furthermore, the EpiIntestinal™ model is commercially available and can be readily sourced in Europe, the US and Asia, making it a valuable model for use in both research and regulatory studies. However, like many other in vitro models, the lack of intestinal peristalsis, digestive fluid, mucous layer and microflora are limitations[26].

2.0 Materials and Methods

2.1 Chemicals

All chemicals were obtained from Sigma Aldrich unless otherwise specified.

2.2 Nanoparticle characterization

SiO_2 (Harvard repository, USA), and Ag NPs (Nanocomposix, USA) were characterized for their pristine size and morphology using a transmission electron microscope (TEM JEOL 2010 HR & UHR) at an accelerating voltage of 200 kV. The elemental composition of NPs was further identified by Energy Dispersive Spectroscopy (EDS; EDAX, USA) mediated compositional analysis.

2.3 Determination of $DSE_{(CRIT)}$

The critical delivered sonication energy (DSE_{CRIT}), which is the minimum required energy per dispersion volume (J/ml) to achieve the smallest possible agglomerates, was determined for each NP type by incremental sonication and size characterization. Suspensions of the NPs in deionized (DI) water were dispersed using a probe sonicator that was first calibrated to determine its energy delivery rate (i.e., Js^{-1}). The mean hydrodynamic diameter of the suspension over time was measured by dynamic light scattering (DLS) and plotted to determine the minimum sonication time and thus energy required to achieve the smallest possible diameter agglomerates. All measurements were performed in triplicate, at 25 °C, using disposable optical polystyrene micro-cuvettes.

2.4 NPs Solubility

NPs suspension (15 mg/ml) were prepared by sonication at DSE_{CRIT} and diluted to 1 mg/ml concentration in water, 3D EpiIntestinal™ tissue medium (SMI-100) and Dulbecco's modified eagle medium (DMEM). The suspensions were incubated at 37°C under ambient conditions for 24 hours, following which any undissolved NPs were removed using high speed centrifugation (25000 g, 15 mins) followed by filtration through a 0.25 µm pore size filter

(Merck Millipore, USA), prior to Inductively Coupled Plasma Optical Emission Spectrometry (ICP-OES) analysis. This was followed by quantification of the amount of dissolved ions.

2.5 Dosimetry

The In vitro Sedimentation, Diffusion and Dosimetry (ISDD) model was followed for performing particle dosimetry [29,30]. The effective density was derived using the volumetric centrifugation method described by DeLoid et al: 1 ml of 1 mg/ml suspension of NPs in SMI-100 and DMEM was kept in packed cell volume (PCV) tubes (Techno Plastic Products (TPP), Trasadingen, Switzerland) and centrifuged in bench-top swing-out rotor centrifuge at 2000g for 1 hour[31]. From the pellet obtained, the volume of the agglomerate pellet (V_{pellet}) was measured with the help of a slide-rule-like easy measure device which was also provided by the PCV tube manufacturers. The Vpellet value was used to determine the effective density (ρEV) using Equation (1) as follows:

$$\rho EV = \rho media + [\left(\frac{Menm}{Vpellet\ .\ SF}\right)\left(1 - \left(\frac{\rho Media}{\rho ENM}\right)\right] \quad (1)$$

where ρmedia is the density of media, Menm is the mass of NPs, Vpellet is the volume of the pellet, SF is the stacking factor and ρENM is the density of pristine NPs. The effective density was calculated for the test NPs in SMI-100 and MEM. Using this effective density, the fraction of particles sedimented (fD) over different time period was determined via MATLAB simulation. fD was then used to calculate the time weighted average dosage.

2.6. *In vitro* cell and tissue culture

(i) 2D cell culture

Caco-2 cell lines, purchased commercially (HTB-37™, American Type Culture Collection ATCC, Manassas, VA) were maintained in complete media MEM supplemented with L-glutamine and 20% fetal bovine serum in 37°C, 5% CO_2. Cells were cultured for at least 2 passages after initiation from liquid nitrogen storage before assay use.

(ii) 3D tissue culture

3D EpiIntestinal™ tissue (SMI-200-FT v2.0) was purchased from MatTek Corporation® (Ashland, MA). The model incorporates enterocytes, paneth cells, M cells, tuft cells and intestinal stem cells into a highly differentiated, polarized epithelium, as described in detail elsewhere[32]. The tissues were processed as instructed by the supplier, treated with test NPs at the concentrations reported in the Results section and maintained with SMI-100-MM culture media at the air-liquid interface at 37°C, 5% CO_2/95% air and 98% relative humidity.

2.7 Tissue barrier integrity assessment

3D intestinal tissues were apically treated with test materials every 24 hours, for a total of 72 hours, prior to assessment of barrier integrity.

FITC-dextran tissue permeability assay:

Changes induced to the barrier function of the EpiIntestinal™ tissues were monitored using fluorescein isothiocyanate (FITC)-dextran 20 kDa (FD20, Sigma Aldrich, St Louis, MO) tissue permeability assay. The tissue permeability was measured in EpiIntestinal™ tissues after adding 3 mg/ml of FD20 to the apical culture media and incubating at 37˚C, for 2h in 5% CO_2/95% air. Tissue permeability was calculated based on the measured Fluorescence Intensity (FI) of FD 20 in the basolateral medium compartment of the 3D cultures, using a microplate reader (Envision, Perkin Elmer, Waltham, MA) at 485/530 nm. FD20 permeation

from the donor medium to the receiver medium was normalized to FD20 that permeated through blank inserts, using Equation (2) as follows:

$$Tissue\ Permeability\ (\%) = \frac{FI\ (basolateral, Tissue) - FI\ (Blank)}{FI\ (basolateral, Blank) - FI\ (Blank)} \times 100 \quad (2)$$

where, *FI (basolateral, Tissue)* represents the measured FD20 fluorescence intensity in the basolateral compartment of the tissue-containing wells; *FI (basolateral, Blank)* represents the measured FD20 fluorescence intensity in the basolateral compartment of the blank inserts; *FI (Blank)* represents the background fluorescence of the medium alone. Tissue barrier integrity was considered uncompromised if FD20 permeability was less than 4%.

Transepithelial electrical resistance (TEER) measurement:

Changes in barrier integrity of the EpiIntestinal™ tissues were assayed using *TEER* with an EVOM volt-ohmmeter equipped with an EndOhm electrode chamber (World Precision Instruments, Sarasota, FL), according to the manufacturer's published protocols. Raw resistance values (Ω) were converted to TEER readings (Ω*cm^2) by multiplying the raw measurements of each tissue by the surface area of the cell culture inserts (0.6 cm^2).

2.8 Tissue dissociation

3D intestinal tissues were dissociated using human tumour dissociation kit (Miltenyl Biotec, Bergisch Gladbach, Germany), as per manufacturers' instruction, with minor modifications. Individual 3D tissues were excised from the culture inserts and incubated for 15 min in cell recovery solution (Corning, Tewksbury, MA). The tissues were subsequently peeled off from

the membrane with fine point forceps. The peeled tissues were placed into gentle MACS C-tube (Miltenyi Biotech, Bergisch Gladbach, Germany) containing the enzyme mix described in the kit's protocol. The tubes were then transferred into a gentleMACS octo dissociator with heater (Miltenyi Biotech, Bergisch Gladbach, Germany), and subjected to one cycle of '37C_m_LPDK_1' program. Upon completion, the cell suspension was centrifuged at 1000 rpm for 5 min; the supernatant was removed, and the pellet was resuspended in 2 ml of Hanks Balanced Salts Solution (HBSS) +Ca/Mg. Total cell number was estimated through cell counting with hemocytometer. The cells were then fixed for micronuclei cytome scoring.

2.9 Micronucleus (MN) cytome assay in 3D EpiIntestinal™ tissue

The MN cytome assay, RICyt, was performed as reported earlier[33]. Tissues were repeatedly exposed to test substances over a period of 10 days, harvested and dissociated into single cell suspension as described above. Cell suspension samples was fixed in Carnoy's solution with 3 fixation steps in methanol/acetic acid 16:1, supplemented with 4% v/v formaldehyde. The cell suspension was aged at least overnight at 4°C to improve the quality of fixed cells. The fixed cells were stained with acridine orange and immediately scored. Cells were scored per criteria originally described by Tolbert *et al*.[34] and Thomas *et al*.[35] One thousand total cells were scored per microtissue to determine the frequency of MN and cytome. The percentage of MN and cytome at each concentration of test chemical was compared with the solvent control. The results were generated from three independent experiments. Each experiment consisted of a single microtissue per dose.

2.10 Comet assay in *in vitro* 3D EpiIntestinal™ tissue

Comet assay was performed as described by Hughes et al[36]. In brief, the apical media was replaced with fresh media containing test materials of interest dispersed in solvent. Tissues were incubated for 24 hours before they were again rinsed and replenished with fresh apical media containing test material. 21 hours after first exposure, tissues were rinsed and dosed again for a final 3 hours before harvesting for comet assay. The total treatment time was 48 hr. At end of exposure, tissues were dissociated and isolated cells were mixed with low melt agarose (LMA) then transferred to each of the two spots on agarose pre-coated glass slides. Slides were cooled to allow LMA to solidify. Cell lysis was carried out by incubating the slides in pre-chilled lysis buffer. For DNA unwinding, slides were then incubated in alkali DNA unwinding solution at room temperature for 20 minutes and electrophoresis was carried out for 30 minutes at 21 V (1V/cm) in electrophoresis buffer using an electrophoresis chamber (4250-050-ESK, Trevigen, Gaithersburg, MD). The electrophoresis tank and solution were pre-chilled for several hours in a cold room prior to usage and electrophoresis was performed in cold room conditions. After electrophoresis, slides were immediately neutralized in distilled water and then twice further for 10 minutes, before being dehydrated in ethanol. Slides were then left to dry overnight at room temperature. DNA was stained with SYBR Green, excess stain was removed and slides were left to dry before they were ready for analysis. Samples were scored and analyzed using a Metafer v3.13.3 scoring platform (Metasystems, Germany). DNA damage was measured and reported as median % tail DNA per microtissue, a minimum of 100 viable comets per tissue. The results for comet assay were generated from three independent experiments. Each experiment consisted of a single microtissue per test concentration.

2.11 Micronucleus assay in Caco-2 cell line

For each treatment assay, cells were seeded at a seeding density of 2 x 10^5 cells/dish in 60mm culture dishes and for 24 h prior to exposure of test materials in MEM with 5% FBS. Each treatment was repeated in duplicates. Caco-2 cells were incubated with the test materials for 24 h and at the end of the treatment, the cells were gently washed twice in PBS and treated with 4.5 µg/ml cytochalasin B (cyto B; Wako Chemicals, Fujifilm) for 29 h. Following which, the cells were washed twice in PBS and replaced with fresh culture media containing 20% FBS for a recovery period of 1.5 h. Cells were then harvested with 0.25% trypsin-EDTA, exposed to cold hypotonic solution (75 mM KCl) and immediately centrifuged to collect the cell pellet. Cells were then resuspended and fixed first in fixative solution of cold methanol/acetic acid (3:1 [v/v]) diluted 1:1 in MEM culture media (20% FBS) and subsequently in undiluted fixative solution. Cells were centrifuged at 1000 rpm for 8 mins after each fixation step. Finally, cells were resuspended in the fixative solution and stored at 4°C. For slide preparations, the cells were spread onto clean glass slides and heat fixed at 51°C on a hot plate for 15 mins. After heat fixing, the cells were stained in 40 µg/ml acridine orange solution and analysed under fluorescence microscope. Micronuclei was performed according to criteria set out in OECD guidelines TG487. Results were taken from 3 independent assay runs.

2.12 Hyperspectral Imaging

Hyperspectral images were obtained and analyzed using the CytoViva® hyperspectral imaging (HSI) microscopy system coupled with the environment for visualizing images (ENVI) software. Spectral acquisition, HSI recording, and spectral mapping analysis were performed according to the Cytoviva® hyperspectral user manual. Prior to HSI analysis of the tissue samples, SiO_2 and Ag NPs were drop casted onto separate slides and mounted with a glass cover slip for HSI acquisition to create individual spectral libraries (SL). After which, HSI images

were recorded for non-treated and treated tissue samples. The spectral angle mapper (SAM), a classification algorithm, was applied to the HSI scans to map spectral similarities between the SLs of SiO_2/Ag NPs and tissue HSI scans. The SAM classification creates two output images: the SAM image of the tissue highlights the pixels that are matched with the applied SL, while the Rule image depicts how each pixel of the input image matches the endmember spectrum in grey scale.

2.13 Tissue sectioning and visualization by transmission electron microscopy (TEM)

To evaluate the localization of the NPs inside the cellular organelles, TEM was carried out. Briefly, the treated and untreated cells and tissues were fixed with a mixture of 4% paraformaldehyde and 2% glutaraldehyde solution overnight at room temperature (RT). They were post-fixed with 2% osmium tetroxide (Sigma Aldrich, USA) for 1 hour and washed with PBS to remove the fixative. Dehydration of cells was done with an ascending series of ethanol (25%, 50%, 75%, 95%, 100%) and pure acetone (100%) for 15 min each at RT. The cells and tissues were then infiltrated with a mixture of epoxy resin (Araldite 502 kit, Ted Pella, USA) and acetone at the ratio 1:1 for 30 min and 1:6 overnight. Each cell pellet and tissue were embedded in fresh resin within a polyurethane mould and polymerized for 48 hours at 60°C. The resulting resin-embedded cell capsules were sectioned at a thickness of 80–100 nm with an ultramicrotome and collected on copper grids. The sections were stained with 2% uranyl acetate for 8 min and lead citrate for 2-3 min before imaging (TEM JEOL 2010 HR & UHR) at an accelerating voltage of 200 kV.

2.14 Statistical Analysis

All quantitative results are presented as mean ± SD and represent a minimum of three independent experiments of n=3, unless otherwise stated. Comparison of means between two sample groups was determined by the two-tailed, unpaired Student's t-test while that for more than two sample groups was done with two tailed one-way ANOVA, and differences are considered significant if $p < 0.05$.

3.0 Results

3.1 Characterization of NPs

The electron micrographs of SiO_2 and Ag NPs are shown in Figure 1. The pristine sizes of the SiO_2 and Ag NPs are 22.1 ± 4.6 nm and 80.1 ± 8.3 nm, respectively, based on image analysis of TEM micrographs. EDX analysis, performed to verify the purity of these NPs, indicated the presence of well-defined elemental peaks for each NPs. Carbon and Copper peaks were detected due to the use of copper grids with lacey carbon for imaging. In addition to the pristine sizes, the hydrodynamic size of SiO_2 NPs was also examined in water (Figure 2A). The critical delivered sonication energy (DSE_{CRIT}) of SiO_2 NPs, was determined to be 235 J/ml. The calculated values for DSE for the different configurations of sonication and time for 15 ml NPs suspension are shown in supplementary Table 1. Sonicating the NPs at their DSE_{CRIT} would provide material-specific amount of acoustic power to break down particle agglomerates at the smallest and most uniform possible hydrodynamic size distribution[37], which allows the stabilization of these NPs in the different cell culture media used in the subsequent in vitro studies. This stabilization was evidenced from the dynamic light scattering (DLS) analysis that recorded NPs hydrodynamic size distribution and poly-dispersity indices, which remain relatively unchanged up to 10 days post dispersion in water (Figure 2B). Additional dispersion

step was not needed for Ag NPs as these were supplied as a fully dispersed solution in citrate buffer.

3.2 Examining the ionic solubility of SiO_2 and Ag NPs in water and tissue culture media

The dissolution both NPs were investigated in water and different culture media – SMI-100 and MEM at concentrations ranging from 1 ppm to 500 ppm (Figure 3). SiO_2 NPs showed very low levels of solubility in water (<1%), but increased dissolution (~30%) in SMI-100 and MEM media at up to 100ppm administered concentration. Ag NPs showed significantly higher dissolution at about 25% in water, 45% in SMI-100 and 55% in MEM media, over the same administered concentration range.

3.3 Dosimetric analysis

The effective densities for both NPs in different culture media were measured using the volumetric centrifugation method[31]. The hydrodynamic size of dispersed particles and their effective densities allows to estimate the fraction of administered dose (fD) that would deposit on cells as a function of time (Figure 4). After 24 hours of incubation in both SMI-100 and MEM medium, approximately 30% to 40% of the administered SiO_2 NPs would be delivered to the cells. Although 100% of the Ag NPs would be delivered to the cells in SMI-100 media after 24 hours of incubation, deposition is slower in MEM medium, resulting to only 50% deposition in 24 hours. This information is used to ensure standardized amount of delivered dose of NPs between different culture formats and media utilized in the study.

3.4 Effect of NPs on barrier integrity of 3D EpiIntestinal™ tissue

The capacity of NPs to induce permeabilization to 3D EpiIntestinal™ tissue was assessed by measuring both FITC-dextran paracellular transport (Figure 5A) and TEER (Figure 5B). Incubation of the tissue in the presence of 50 µg/ml FITC-dextran in the apical chamber did not cause any increase in FITC-dextran paracellular transport nor any decrease in TEER values. These results confirm that under the existing experiment conditions, the tested NPs did not affect the permeabilization of 3D EpiIntestinal™ tissue. The tissue barrier remained intact following SiO_2 and Ag NPs exposure. Cytochalasin B (Cyto B) at 20 µg/ml was used as positive control to ensure validity of both assays. Addition of Cyto B caused a significant increase in FITC-dextran paracellular transport (25%, $p < 0.05$) and a significant decrease in TEER value (68%, $p < 0.05$).

3.5 Genotoxicity assessment of NPs in *in vitro* 3D EpiIntestinal™ tissue

The genotoxic potential of the tested NPs in 3D EpiIntestinal™ tissue was investigated through the newly developed reconstructed micronuclei cytome (RICyt) assay protocol[33]. Micronuclei (Figure 6) alongside with other cell types and nuclei anomalies (Table 1) were scored for genotoxicity assessment. Neither genotoxicity nor cytotoxicity were detected in tissues exposed with SiO_2 NP (Figure 6A) and Ag NP (Figure 6B). Other than micronuclei, the tested NPs also did not induce other forms of nuclear anomalies as depicted in Table 1. Solvent controls, 10% H_20 and 5% citrate buffer, produced low level of basal micronuclei frequency (~1.2-1.5%). The positive control, mitomycin C at 1 µg/ml, consistently produced ~2.2-fold increase ($p < 0.05$) in micronuclei production and 8.12% increase ($p < 0.05$) in karyorrhexis (i.e., apoptosis).

The NPs were also tested using the reconstructed intestine comet (RICom) assay protocol. For both NPs two tailed one-way ANOVA showed no statistically significant difference

between groups for % tail DNA and no values were above the upper historical negative control range (5.16%), with minimal accompanying cytotoxicity. A clear negative result (Figure 7, Table 2) was shown. The positive control, ethyl methanesulfonate at 500 µg/ml, consistently produced a significant difference in % tail DNA ($p < 0.05$).

Table 1. Comet genotoxicity assessment of NPs in 3D EpiIntestinal™ tissue. Tissues were exposed to test articles for 2 days via apical treatment. At the end of treatment, tissues were dissociated to single cells for comet slide preparation. One hundred viable comets were scored per microtissue to determine the median % tail DNA. The mean % tail DNA from three independent experiments are shown. +ve control; 500 µg/ml ethyl methanesulfonate. * $p < 0.01$ in two tailed one-way ANOVA with Tukey's post-hoc test, relative to other sample groups in the corresponding series.

Test Material	Test concentration (µg/ml)	Tail DNA %		Relative Cell Count %	
		Mean	STDEV	Mean	STDEV
SiO_2 NP	solvent	2.46	0.65	100.00	0.00
	25.0	3.22	0.68	98.30	0.30
	50.0	2.29	0.59	96.71	9.46
	100.0	2.28	0.23	82.56	10.38
	+ve control	29.17 *	2.96	93.96	44.41
Ag NP	solvent	1.85	0.49	100.00	0.00
	25.0	2.69	0.44	83.00	7.94
	50.0	2.18	0.80	90.65	11.37
	100.0	3.11	0.47	83.76	21.11
	+ve control	30.89 *	2.45	86.10	14.38

SiO_2 NP: silicon dioxide nanoparticles; AgNP: silver nanoparticles.

Table 2. Frequencies of cell types and nuclear anomalies in scored in 3D EpiIntestinal™ tissue. Nanoparticles were applied to the apical surface of 3D EpiIntestinal™ tissues for 10 days.

Tissues were dissociated into single cell suspensions and fixed in Carnoy's fixative. One thousand total cells were scored per microtissue to determine the frequency of MN and cytome induction. The results from three independent experiments are shown. Each experiment consisted of a single microtissue per test dose. Mitomycin C (1 µg/ml) were used as positive control. Water (10%) and citrate buffer (5%) were solvent controls. Data are reported as percentage (mean ± SD). $*p < 0.05$; $**p < 0.001$ compared with other MN % sample groups in the corresponding series.

SiO_2 NP (µg/ml)	MN	Buds	Mono	BN	CC	KR	PY	KL
10% H2O	1.47 ± 0.03	0.40 ± 0.10	92.10 ± 1.36	0.87 ± 0.24	0.20 ± 0.12	3.87 ± 0.71	0.40 ± 0.25	0.70 ± 0.06
1	1.50 ± 0.12	0.30 ± 0.15	93.57 ± 1.32	0.73 ± 0.32	0.10 ± 0.10	3.00 ± 0.70	0.40 ± 0.12	0.40 ± 0.25
10	1.90 ± 0.06	0.57 ± 0.09	90.9 ± 0.76	1.13 ± 0.20	0.13 ± 0.07	3.80 ± 0.35	0.77 ± 0.33	0.80 ± 0.15
50	1.76 ± 0.14	0.60 ± 0.15	90.31 ± 2.01	0.93 ± 0.33	0.23 ± 0.19	4.60 ± 0.97	0.53 ± 0.27	1.03 ± 0.49
MMC 1 µg/ml	3.13 ± 0.26**	0.93 ± 0.07	85.17 ± 1.28	1.33 ± 0.12	0.13 ± 0.09	8.40 ± 1.33	0.53 ± 0.33	0.37 ± 0.07

AgNP (µg/ml)	MN	Buds	Mono	BN	CC	KR	PY	KL
Citrate buffer	1.63 ± 0.19	0.57 ± 0.19	92.77 ± 1.05	1.07 ± 0.38	0.07 ± 0.03	3.07 ± 0.22	0.67 ± 0.33	0.17 ± 0.09
1	1.87 ± 0.32	0.47 ± 0.18	92.73 ± 0.73	0.97 ± 0.15	0.07 ± 0.07	2.77 ± 0.27	0.57 ± 0.09	0.57 ± 0.13
10	1.77 ± 0.32	0.27 ± 0.07	94.14 ± 1.00	1.07 ± 0.19	0.03 ± 0.03	1.93 ± 0.41	0.47 ± 0.29	0.33 ± 0.23
50	1.57 ± 0.27	0.33 ± 0.15	93.93 ± 0.86	1.10 ± 0.21	0.07 ± 0.07	2.43 ± 0.79	0.33 ± 0.03	0.23 ± 0.03
MMC 1 µg/ml	3.13 ± 0.26*	0.93 ± 0.07	85.17 ± 1.28	1.33 ± 0.12	0.13 ± 0.09	8.40 ± 1.33	0.53 ± 0.33	0.37 ± 0.07

MN, micronuclei; Buds, nuclear buds; Mono, mononucleated cells (basal and differentiated); BN, binucleated cells; CC, condensed chromatin; KR, karyorrhexis; PY, pyknosis; KL, karyolysis

3.6 Genotoxicity assessment of NPs in *in vitro* 2D Caco-2 cells

The selected nanomaterials were assessed for genotoxicity in Caco-2 colon cell line with the cytokinesis-blocked micronucleus assay protocol according to OECD TG487 guidelines. Both NPs did not induce significant micronuclei numbers and cytotoxicity compared to the solvent control (Figure 8, Table 3). For the samples tested with Ag NPs standard (NanoComposix, Ag75, AGCO75), Caco-2 showed significant dose dependent cytotoxicity ($p < 0.0001$) compared with the solvent control. However, there were no significant genotoxicity detected across the treatment groups.

Table 3. Frequency of micronucleus scored in Caco-2 cells treated with A. SiO_2 NP and B. Ag NP. The results from three independent experiments are shown. Mitomycin C (0.03 µg/ml) were used as positive control. Water (10%) and citrate buffer (10%) were solvent controls. The values are expressed as percentages compared to solvent controls and presented as mean ± SD.

A. SiO_2NP, E551 (µg/ml)	**% MN**	**% Cell Viability**
10% H_2O	2.99 ± 0.49	100 ± 0.00
1	2.89 ± 0.94	96.78 ± 0.98
10	3.26 ± 0.53	98.63 ± 6.96
50	3.49 ± 0.83	98.33 ± 8.48
MMC (µg/ml)	**% MN**	**% Cell Viability**
0.03	10.68 ± 0.41	85.61 ± 10.28

B. AgNP, AGC075 (µg/ml)	% MN	% Cell Viability
10% Citrate Buffer	3.66 ± 1.11	100 ± 0.00
1	5.13 ± 2.43	86.17 ± 6.35
2	5.65 ± 1.93	55.69 ± 3.21
MMC (µg/ml)	**% MN**	**% Cell Viability**
0.03	13.14 ± 4.15	82.15 ± 1.88

3.7 Hyperspectral imaging (HSI) and spectral mapping of NPs-exposed 3D EpiIntestinal™ tissue

Hyperspectral imaging was performed to examine SiO_2 and Ag NP penetration in 3D EpiIntestinal™ tissue. Prior to HSI acquisition of tissues, individual spectral libraries (SL) were obtained for pristine SiO_2 and Ag NPs (supplementary Figure 1A and 1B). Reference spectra collected from SiO_2 NPs had consistent profiles over 450 – 800 nm. In contrast, the spectra collected from Ag NPs showed more varied profiles over the similar range of wavelengths. Next, brightfield and darkfield images were obtained for controls and NPs treated 3D tissues, followed by spectral mapping using the Cytoviva™ ENVI software to identify internalized NPs. Tissue imaging in Citrate buffer (CB) group was included as a control because Ag NPs were suspended in CB.

After 48hours of exposure to 50 µg/ml of SiO_2 NPs, SAM images revealed localized spectral profiles of SiO_2 NPs mainly accumulated at the bottom of the tissue, which was not observed

in the controls (Figure 9). Spectral profile of Ag NPs was less intense but evenly distributed throughout the tissue sample (Figure 9).

3.8 Intracellular localization of NPs in 3D EpiIntestinal™ tissue and 2D Caco-2 gut cell line

To study the internalization, localization and cellular impact of the test NPs on 3D intestinal tissue, TEM was performed. The TEM micrographs indicated internalization of SiO_2 and Ag NPs in both 3D EpiIntestinal™ tissue as well as 2D Caco-2 cells, Figure 10 and Figure 11, respectively. The untreated control (CTR) tissue appeared healthy as evidenced by 1) healthy nuclear morphology with intact nuclear membrane 2) presence of brush border-like morphology, and 3) presence of gap junctions (Figure 10 top panel). Tissues exposed to SiO_2 NPs displayed cytosolic localization of NPs and extensive cytoplasmic vacuolization. Additionally, there was an increase in the number of perinuclear autophagosomes, although no change in nuclear morphology was observed. Like SiO_2, Ag NPs also showed cytosolic localization, however, the nucleus appeared fragmented with increased appearance of micronuclei and autophagosomes around the nucleus. Similar observations were made in 2D cells (Figure 11) where SiO_2 caused formation of large cytoplasmic vacuoles. Although Ag NPs uptake was much lower compared to SiO_2, the cellular damages observed were more significant. Furthermore, elemental mapping performed with Scanning-TEM (STEM) in Figure 12, showed the presence of Si and Ag, as depicted by the red channels, inside the cells, confirming the corresponding uptake of NPs by the cells.

4.0 Discussion

This study compared two in vitro models—2D Caco-2 cells and 3D EpiIntestinal™—to evaluate the impact of food-based NPs: SiO_2 (E551) and Ag (AGCO75) on cellular responses and

genotoxicity in the human gastrointestinal system. The 2D Caco-2 model is appreciated for its simplicity, cost-effectiveness, and ease of use but lacks the physiological complexity and tissue architecture of in vivo conditions. Caco-2 cells are also susceptible to oxidant induced effects and are not necessarily a good model system to investigate toxicity in the gut[38,39]. In contrast, the 3D EpiIntestinal™ model offers a more physiologically relevant context, replicating in vivo tissue structure and cell interactions. it has also been shown that general metabolic capacity is greater in the EpiIntestinal™ model, which more closely resembles metabolic capacity in the gut[39]. Hence, we sought to determine if the EpiIntestinal™ model is a suitable platform for evaluating the toxicity of ingested food-based NPs, particularly in the context of genotoxicity, using adapted test protocols.

Before delving into cellular responses, it is crucial to address various factors influencing the behavior of NPs in physiological environment. These factors include chemical composition, size, shape, charge, surface area and hydrophobicity. The physicochemical and colloidal properties of NPs play a pivotal role in governing their nano-bio interactions with cells and surrounding tissues. Therefore, it is imperative to have well-characterized and stable colloidal NPs to ensure reproducibility in nanotoxicological studies. To attain this, a comprehensive characterization of these factors was performed. Additionally, an integrated method, previously developed by DeLoid et al., was also employed in this study. This method involves dispersing the NPs, characterizing their colloidal stability, and estimating the delivered dose for subsequent in vitro studies[31]. Through the application of this model, respective delivered dosage of a stable NPs dispersion was exposed to the 3D tissue and Caco-2 cell line.

Upon exposure of NPs to the intestinal tissue, the tissue's barrier integrity was examined to investigate the interaction between NPs and biological barriers of the tissue. We evaluated the capacity of NPs to induce permeabilization by measuring both FITC-dextran paracellular

transport and TEER. Interestingly, incubation of the tissue with NPs, specifically at a concentration of 50 µg/ml, did not result in any significant increase in FITC-dextran paracellular transport or decrease in TEER values. The intactness of the tissue barrier following exposure to NPs suggest that under the tested conditions, both NPs did not disrupt the integrity of 3D EpiIntestinal™ tissue barrier. This is particularly significant in the context of NP toxicity assessment, as disruptions in epithelial barriers could lead to increased absorption of NPs and potentially adverse effects. To validate the reliability of the assays used in this study, Cytochalasin B (Cyto B), a known disruptor of the cytoskeleton and inducer of permeabilization, was employed as a positive control. As expected, addition of Cyto B resulted in a significant increase in FITC-dextran paracellular transport and a substantial decrease in TEER value, confirming the sensitivity and validity of both assays.

Next, we investigated the cytotoxicity and genotoxicity induced by these NPs in 3D intestinal tissue and Caco-2 cell line. The findings from micronuclei cytome (RICyt) assay indicated that neither SiO_2 nor Ag NPs induce genotoxicity nor cytotoxicity in dosed 3D EpiIntestinal™ tissue. This observation was further supported by the absence of other nuclear anomalies apart from micronuclei. Additionally, the solvent controls produced only a low level of basal micronuclei frequency, confirming the validity of the assay. The positive control, mitomycin C, demonstrated the assay's sensitivity by inducing a significant increase in micronuclei production and karyorrhexis. Furthermore, the reconstructed intestine comet (RICom) assay protocol also yielded negative results for both SiO_2 and Ag NPs, with no statistically significant increase in % tail DNA observed above historical negative control range, and minimal accompanying cytotoxicity. The genotoxicity findings in the 3D EpiIntestinal™ platform is reproducible in OECD recommended cell line, Caco-2, and in line with published literature. Consistent with the findings in the 3D EpiIntestinal™ tissue model, neither SiO_2 NPs nor Ag

NPs induced significant micronuclei formation or cytotoxicity compared to the solvent control in the 2D Caco-2 cultures. However, it is important to note that the Ag NPs standard exhibited significant dose-dependent cytotoxicity in Caco-2 cells, although no significant genotoxicity was detected across the treatment groups. This could be explained by the intactness of the 3D intestinal tissue barrier upon exposure of the Ag NPs, compared to 2D cultures. This barrier effect may be providing a protective effect, limiting exposure of cells to exogenous generation of ROS[39]. Overall, the results from both the 3D EpiIntestinal™ tissue model and the 2D Caco-2 colon cell line suggest that the tested NPs, SiO_2 and Ag, do not present genotoxic and intestinal barrier dysfunction risks to the human gut under the tested conditions, although a dose-dependent Ag NP induced reduction in cell viability was observed in Caco-2 cells.

In addition to assessing genotoxicity, HSI and TEM were employed to investigate the potential of SiO_2 and Ag NPs to penetrate the tissue layers and cellular uptake. These complementary techniques provide valuable insights into the interactions between NPs and biological tissues, shedding light on their distribution and localization within cellular compartments. By examining the spatial distribution of NPs within the tissue layers and characterizing their cellular uptake, we can further elucidate the mechanisms underlying the biological effects observed in our genotoxicity assessments. Both SiO_2 and Ag NPs were internalized by the 3D EpiIntestinal™ tissues and localized in the cytosolic region. HSI showed localized spectral profiles of SiO_2 NPs at the bottom of the tissue, whereas even distribution of Ag NPs throughout the tissue indicates differential penetration behaviors between the two NPs within the 3D intestinal tissue. Though internalized, both NPs produce no damaging effects to the barrier of intestinal epithelium, as discussed earlier, suggesting that tight junction proteins are not targeted for their entry into the cells. Further investigation into the intracellular localization and impact of NPs was conducted using TEM. Both SiO_2 and Ag NPs

were found to be internalized by the cells in 3D tissue as well as in 2D cell models. The tissues exposed to SiO_2 NPs displayed cytosolic vacuolization and an increase in perinuclear autophagosomes. Similarly, Ag NPs exhibited cytosolic localization, yet induced nuclear fragmentation, micronuclei formation, and increased autophagosome, suggesting more pronounced cellular damage compared to SiO_2 NPs. This phenomenon could be due to the oversaturation or off-target effect from high dose of both NPs (50 µg/ml) added to the tissues. The presence of autophagosomes infers potential autophagic processing of NPs and could be essential for maintenance of intestinal epithelial cell integrity and subsequent lysosomal exocytosis of the NPs[40]. In comparison, Caco-2 cells treated with SiO_2 NPs exhibited the formation of large cytoplasmic vacuoles, while Ag NPs induced lower cell uptake but more significant cellular damage. Elemental mapping with scanning-TEM (STEM) confirmed the presence of Si and Ag elements inside the cells, further validating NP uptake.

Earlier, there have been several studies carried out to investigate possible genotoxic effects of SiO_2 and Ag NPs. Negative findings were observed in in vitro studies evaluating SiO_2 NPs induced DNA fragmentation in comet assay[41], chromosomal aberrations, and micronuclei[42]. In vivo studies also showed negative findings in comet assay in duodenum and colon in rats, following oral route of exposure[43], in agreement with a separate study that indicated SiO_2 NPs had a low potential to cross the gastrointestinal tract[44]. Overall, SiO_2 NPs used as a food additive did not raise concerns with respect to genotoxicity[45]. In animal studies with oral acute exposure in adult mice, Ag NPs were mostly accumulated in duodenum. Localization analysis showed that Ag NPs scatter in cytoplasm or membrane bound organelles but never in the nucleus, accounting for the lack of genotoxicity evaluated by comet or micronucleus assay[46]. It was concluded that the use of the Ag NPs as an additive at up to 0.025% w/w in food contact

material does not raise safety concerns for the consumer[47]. The genotoxicity data in 2D and 3D models from our study are in line with and supported by these published findings.

5.0 Conclusion

The integration of 3D intestinal tissue models and 2D Caco-2 gut cell line models provides a comprehensive approach to understanding the behavior of food-based NPs. By combining these models, we can overcome limitations and gain a nuanced perspective on NP interactions. This approach is crucial for accurately predicting NP toxicity in the food industry. Utilizing complementary 2D and 3D assays allows for initial genotoxicity assessment in 2D models, followed by validation in 3D models simulating relevant exposure routes, such as the intestinal route. In this study, by using both 2D Caco-2 cell cultures and 3D EpiIntestinal™ small intestinal microtissues, we found that neither genotoxicity nor cytotoxicity were detected in the 3D tissues after SiO_2 and Ag NP treatment, while the 2D cultures exhibited cytotoxic response from Ag NP treatment. Both NPs were internalized into cells in both 2D and 3D culture models. Overall, the 3D small intestinal tissue model was found to be more resilient to NP treatment compared to 2D Caco-2 cell monolayers. Moving forward, the development and validation of 3D models will enhance predictive capabilities and improve prioritization of animal testing based on exposure risk. While the EpiIntestinal™ microtissues system shows promise as an initial testing platform, further validation is needed for accurate toxicity prediction. Continued research in this area will advance our understanding of NP interactions in gastrointestinal contexts, leading to safer food-based nanoparticle products and enhanced consumer safety.

6.0 Acknowledgment

This research was supported by the Industry Alignment Fund (Pre-Positioning; IAF-PP-H18/01/a0/G14), Biomedical Research Council (BMRC, A*STAR). The authors acknowledge the Facility for Analysis, Characterization, Testing and Simulation (FACTS), NTU, for the support in electron microscopy analysis.

7.0 References

1. Organization, W. H. Food additives. Preprint at (2022).
2. Ashfaq, A., Khursheed, N., Fatima, S., Anjum, Z. & Younis, K. Application of nanotechnology in food packaging: Pros and Cons. *J Agric Food Res* **7**, 100270 (2022).
3. Onyeaka, H., Passaretti, P., Miri, T. & Al-Sharify, Z. T. The safety of nanomaterials in food production and packaging. *Curr Res Food Sci* **5**, 763–774 (2022).
4. Vance, M. E. *et al.* Nanotechnology in the real world: Redeveloping the nanomaterial consumer products inventory. *Beilstein J Nanotechnol.* **6**, 1769–1780 (2015).
5. Cao, Y. *et al.* Consideration of interaction between nanoparticles and food components for the safety assessment of nanoparticles following oral exposure: A review. *Environ Toxicol Pharmacol.* **46**, 206–210 (2016).
6. Dekkers, S. *et al.* Presence and risks of nanosilica in food products. *Nanotoxicology* **5**, 393–405 (2011).
7. Wang, H., Du, L. J., Song, Z. M. & Chen, X. X. Progress in the characterization and safety evaluation of engineered inorganic nanomaterials in food. *Nanomedicine (Lond).* **8**, 2007–2025 (2013).
8. Barahona, F., Ojea-Jimenez, I., Geiss, O., Gilliland, D. & Barrero-Moreno, J. Multimethod approach for the detection and characterisation of food-grade synthetic amorphous silica nanoparticles. *J Chromatogr A* **1432**, 92–100 (2016).
9. Athinarayanan, J., Periasamy, V. S., Alsaif, M. A., Al-Warthan, A. A. & Alshatwi, A. A. Presence of nanosilica (E551) in commercial food products: TNF-mediated oxidative stress and altered cell cycle progression in human lung fibroblast cells. *Cell Biol Toxicol* **30**, 89–100 (2014).
10. Yoo, N.-K., Jeon, Y.-R. & Choi, S.-J. Determination of two differently manufactured silicon dioxide nanoparticles by cloud point extraction approach in intestinal cells, intestinal barriers and tissues. *Int J Mol Sci* **22**, 7035 (2021).
11. Peters, R. *et al.* Presence of nano-sized silica during in vitro digestion of foods containing silica as a food additive. *ACS Nano* **6**, 2441–2451 (2012).
12. Sukhanova, A. *et al.* Dependence of nanoparticle toxicity on their physical and chemical properties. *Nanoscale Res Lett* **13**, 1–21 (2018).
13. Lamas, B., Martins Breyner, N. & Houdeau, E. Impacts of foodborne inorganic nanoparticles on the gut microbiota-immune axis: potential consequences for host health. *Part Fibre Toxicol* **17**, 1–22 (2020).

14. Murugadoss, S. *et al.* Toxicology of silica nanoparticles: an update. *Arch Toxicol* **91**, 2967–3010 (2017).
15. Napierska, D., Thomassen, L. C., Lison, D., Martens, J. A. & Hoet, P. H. The nanosilica hazard: another variable entity. *Part Fibre Toxicol* **7**, 1–32 (2010).
16. Gaillet, S. & Rouanet, J.-M. Silver nanoparticles: their potential toxic effects after oral exposure and underlying mechanisms--a review. *Food and Chemical Toxicology.* **77**, 58–63 (2015).
17. Istiqola, A. & Syafiuddin, A. A review of silver nanoparticles in food packaging technologies: Regulation, methods, properties, migration, and future challenges. *Journal of the Chinese Chemical Society.* **67**, 1942–1956 (2020).
18. McClements, D. J. & Xiao, H. Is nano safe in foods? Establishing the factors impacting the gastrointestinal fate and toxicity of organic and inorganic food-grade nanoparticles. *NPJ Sci Food* **1**, 6 (2017).
19. Jaswal, T. & Gupta, J. A review on the toxicity of silver nanoparticles on human health. *Mater Today Proc* **81**, 859–863 (2023).
20. Yazdimamaghani, M., Moos, P. J., Dobrovolskaia, M. A. & Ghandehari, H. Genotoxicity of amorphous silica nanoparticles: Status and prospects. *Nanomedicine* **16**, 106–125 (2019).
21. Lee, J., Lilly, G. D., Doty, R. C., Podsiadlo, P. & Kotov, N. A. In vitro toxicity testing of nanoparticles in 3D cell culture. *Small.* **5**, 1213–1221 (2009).
22. Lee, J., Cuddihy, M. J. & Kotov, N. A. Three-dimensional cell culture matrices: state of the art. *Tissue Eng Part B Rev.* **14**, 61–86 (2008).
23. Griffith, L. G. & Swartz, M. A. Capturing complex 3D tissue physiology in vitro. *Nat Rev Mol Cell Biol.* **7**, 211–224 (2006).
24. Helander, H. F. & Fändriks, L. Surface area of the digestive tract - revisited. *Scand J Gastroenterol.* **49**, 681–689 (2014).
25. Egger, L. & others. The harmonized INFOGEST in vitro digestion method: From knowledge to action. *Food Research International* **88**, 217–225 (2016).
26. Temple, J., Velliou, E., Shehata, M. & Lévy, R. Current strategies with implementation of three-dimensional cell culture: the challenge of quantification. *Interface Focus* **12**, (2022).
27. Ahmad, M. K., Khan, A. A., Ali, S. N. & Mahmood, R. Chemoprotective Effect of Taurine on Potassium Bromate-Induced DNA Damage, DNA-Protein Cross-Linking and Oxidative Stress in Rat Intestine. *PLoS One* **10**, e0119137 (2015).
28. Ayehunie, S. *et al.* Human Primary Cell-Based Organotypic Microtissues for Modeling Small Intestinal Drug Absorption. *Pharm Res.* **35**, 72 (2018).
29. Hinderliter, P. M. *et al.* ISDD: A computational model of particle sedimentation, diffusion and target cell dosimetry for in vitro toxicity studies. *Part Fibre Toxicol.* **7**, 36 (2010).
30. Rakshit, M. *et al.* Hydroxyapatite Particles Induced Modulation of Collagen Expression and Secretion in Primary Human Dermal Fibroblasts. *Int J Nanomedicine.* **15**, 4943–4956 (2020).
31. DeLoid, G. *et al.* Estimating the effective density of engineered nanomaterials for in vitro dosimetry. *Nat Commun* **5**, 3514 (2014).
32. Ayehunie, S. *et al.* Novel 3D Human Small Intestinal Tissue Model (EpiIntestinal TM) to Assess Drug Permeation & Inflammation. (2014).

33. Lim, H. K. *et al. Development of Reconstructed Intestinal Micronucleus Cytome (RICyt) Assay in 3D Human Gut Model for Genotoxicity Assessment of Orally Ingested Substances*. (Arch Toxicol, 2022).
34. Tolbert, P. E., Shy, C. M. & Allen, J. W. Micronuclei and other nuclear anomalies in buccal smears: methods development. *Mutat Res.* **271**, 69–77 (1992).
35. Thomas, P. *et al.* Buccal micronucleus cytome assay. *Nat Protoc.* **4**, 825–837 (2009).
36. Hughes, C. O., Lim, H. K., Tan, J. C. W., Leavesley, D. I. & Smith, B. P. C. Reconstructed human intestinal comet assay, a possible alternative in vitro model for genotoxicity assessment. *Mutagenesis* **38**, 139–150 (2023).
37. Cohen, J. M., Beltran-Huarac, J., Pyrgiotakis, G. & Demokritou, P. Effective delivery of sonication energy to fast settling and agglomerating nanomaterial suspensions for cellular studies: Implications for stability, particle kinetics, dosimetry and toxicity. *NanoImpact* **10**, 81–86 (2018).
38. Baker, S. S. & Baker, R. D. Caco-2 cell metabolism of oxygen-derived radicals. *Dig Dis Sci* **38**, 2273–2280 (1993).
39. Markus, J. *et al.* Human small intestinal organotypic culture model for drug permeation, inflammation, and toxicity assays. *In Vitro Cell Dev Biol Anim* **57**, 160–173 (2021).
40. Sipos, A. *et al.* Alveolar epithelial cell processing of nanoparticles activates autophagy and lysosomal exocytosis. Am J Physiol Lung Cell Mol Physiol.
41. Gonzalez, L. *et al.* Exploring the aneugenic and clastogenic potential in the nanosize range: A549 human lung carcinoma cells and amorphous monodisperse silica nanoparticles as models. *Nanotoxicology* **4**, 382–395 (2010).
42. Vecchio, G., Fenech, M., Pompa, P. P. & Voelcker, N. H. Lab-on-a-chip-based high-throughput screening of the genotoxicity of engineered nanomaterials. *Small.* **10**, 2721–2734 (2014).
43. Tarantini, A. *et al.* Genotoxicity of synthetic amorphous silica nanoparticles in rats following short-term exposure. Part 1: oral route. *Environ Mol Mutagen.* **56**, 218–227 (2015).
44. Yang, Y. X. *et al.* Evaluation of the toxicity of food additive silica nanoparticles on gastrointestinal cells. *J Appl Toxicol.* **34**, 424–435 (2014).
45. oFAaNSat, F. Ep. *et al.* Re-evaluation of silicon dioxide (E 551) as a food additive. *EFSA Journal.* **16**, e05088 (2018).
46. Narciso, L. *et al.* Genotoxicity, biodistribution and toxic effects of silver nanoparticles after in vivo acute oral administration. *NanoImpact* **18**, 100221 (2020).
47. Panel, E. on Food Contact Materials EaPA, Lambré C, Barat Baviera JM, Bolognesi C, Chesson A, Cocconcelli PS, et al. Safety assessment of the substance silver nanoparticles for use in food contact materials. *EFSA Journal.* **19**, e06790 (2021).

Assessing nanotoxicity of food-relevant particles: A comparative analysis of cellular responses in cell monolayers versus 3D gut epithelial cultures

Archana Gautam[1 #], Hui Kheng Lim[2,3,4 #], Jasmine Jia'En Li[5 #], Christopher Owen Hughes[2,3,4], Calvin Wee Sing Yeo[5], Moumita Rakshit[1], David Ian Leavesley[3], Michelle Jing Sin Lim[4,6], Joseph Choon Wee Tan[4], Li Yi Tan[1], Joanne Sheot Harn Chan[5], Benjamin Paul Chapman Smith[2,4,6,7 *], Kee Woei Ng[1,3,8 **]

[1]School of Materials Science and Engineering, Nanyang Technological University, 50 Nanyang Avenue, Singapore

[2]Innovations in Food and Chemical Safety (IFCS) Programme, Agency for Science, Technology and Research, Singapore

[3]Skin Research Institute of Singapore (SRIS), Agency for Science, Technology and Research, Singapore

[4]Future Ready Food Safety Hub (a joint initiative of A*STAR, SFA & NTU), Nanyang Technological University, Singapore

[5]National Centre for Food Science, Singapore Food Agency, Singapore

[6]Singapore Institute of Food and Biotechnology Innovation (SIFBI), Agency for Science, Technology and Research, Singapore

[7]Chemical Senses Center, 3500 Market Street, Pennsylvania, 19104, USA

[8]Nanyang Environment and Water Research Institute, Nanyang Technological University, 1 Cleantech Loop, CleanTech One, Singapore

[#] These authors contributed equally to this work

Corresponding authors:

*bsmith@monell.org

**kwng@ntu.edu.sg

Declaration of Interest Statement

The authors declare that they have no known competing financial interests or personal relationships that could have influenced the work reported in this paper.

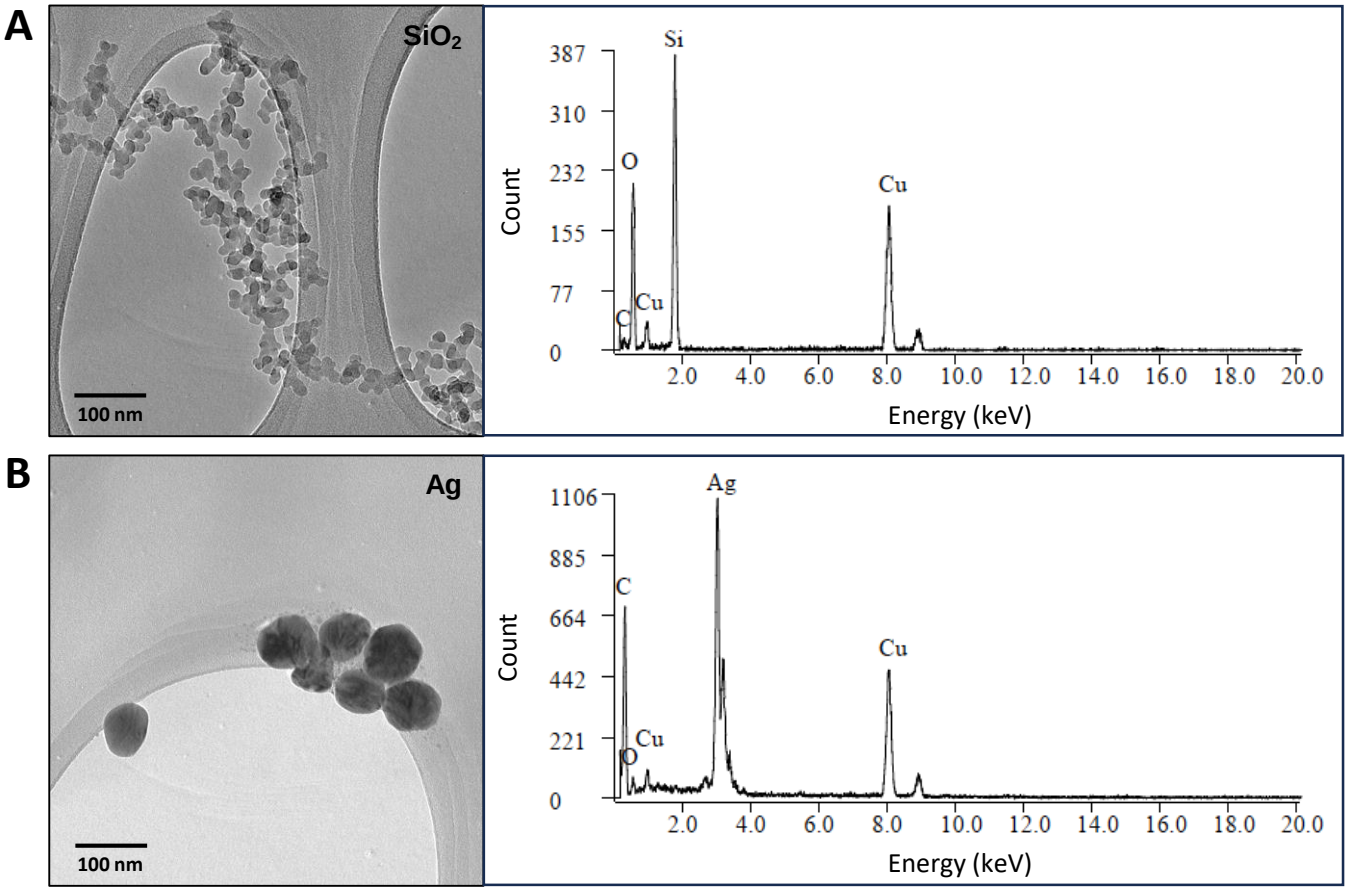

Figure 1. TEM and EDX analysis of SiO_2 and Ag NPs. NPs were drop-cast on lacey carbon copper grids and imaged using high resolution transmission electron microscopy. Figure shows the TEM micrographs with their respective EDX elemental spectrum for (A) SiO_2, and (B) Ag NPs. Scale bar = 100 nm.

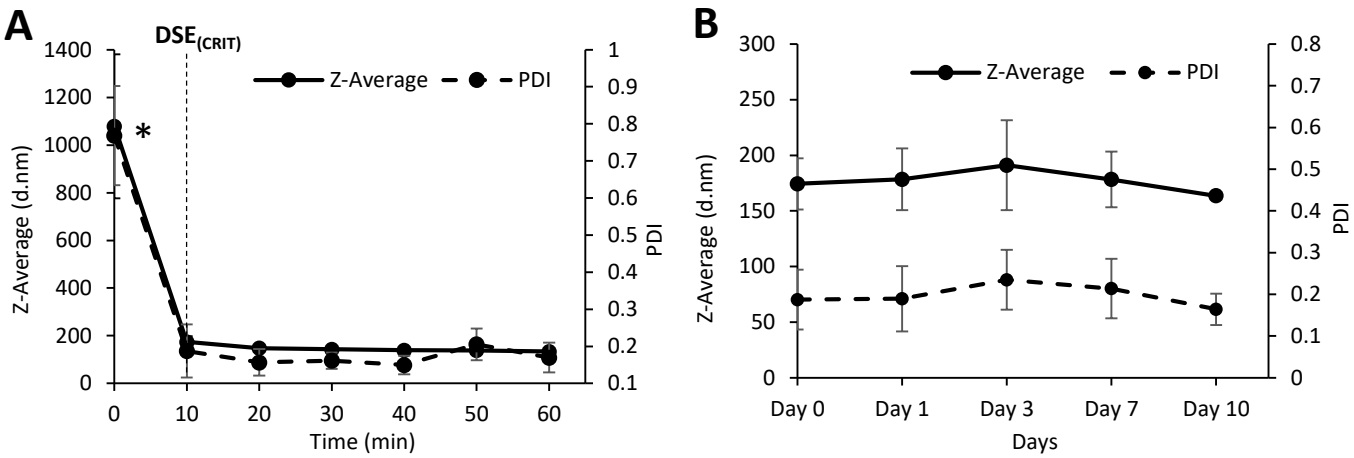

Figure 2. Determination of $DSE_{(CRIT)}$. (A) SiO_2 NPs were suspended in 15ml water at 15mg/ml concentration and sonicated for various time intervals and the average hydrodynamic size (Z-average) and PDI were measured to determine the critical delivered sonication energy ($DSE_{(CRIT)}$). (B) SiO_2 NPs were sonicated at their respective $DSE_{(CRIT)}$ and the Z-average and PDI were monitored over a period of 10 days. Graphs show that the Z-average and PDI remain constant for both NPs over 10 days. Comparison of means was done using one-way ANOVA and Tukey's post hoc test: * $p < 0.05$ compared with other sample groups in the corresponding series. Data is presented as means ± SD; N=3, n=3.

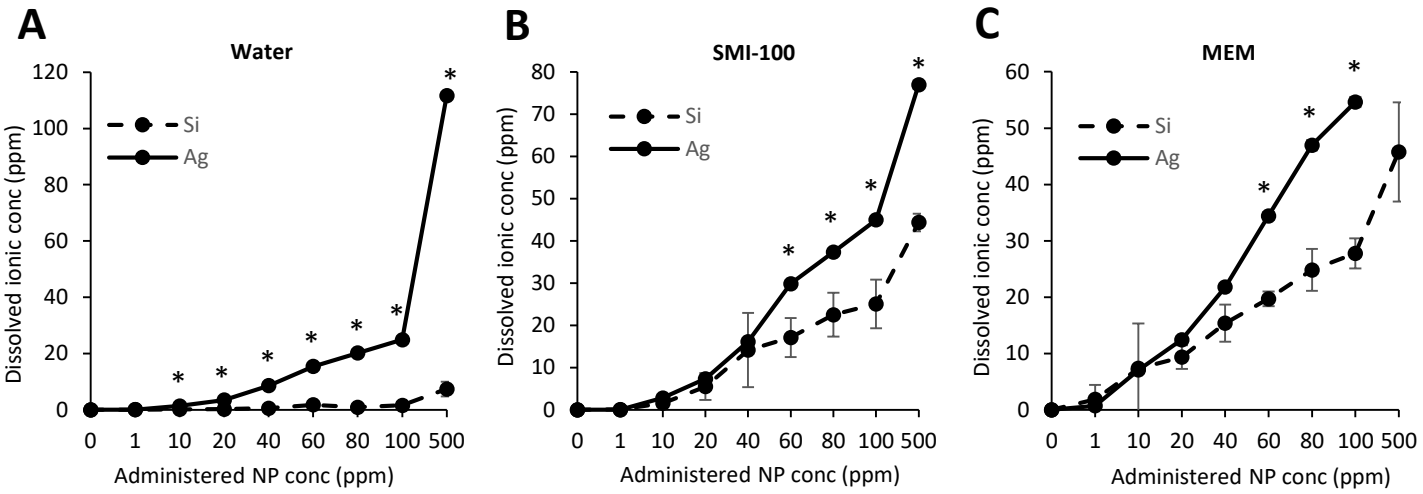

Figure 3. Solubility of NPs in water and media. The NPs were sonicated at their $DSE_{(CRIT)}$ and suspended in water or media (SMI-100 and MEM) at various concentrations. They were incubated at 37 °C for 24 h, followed by centrifugation and filtration. Graphs show the dissolved ionic concentrations (ppm) versus the administered particle concentrations (ppm) in (A) water, (B) SMI-100 and (C) MEM media. Comparison of means was done using unpaired Student's t-test; * $p < 0.05$ comparing between both NPs at each corresponding concentration. Data is presented as means ± SD; N=3, n=3.

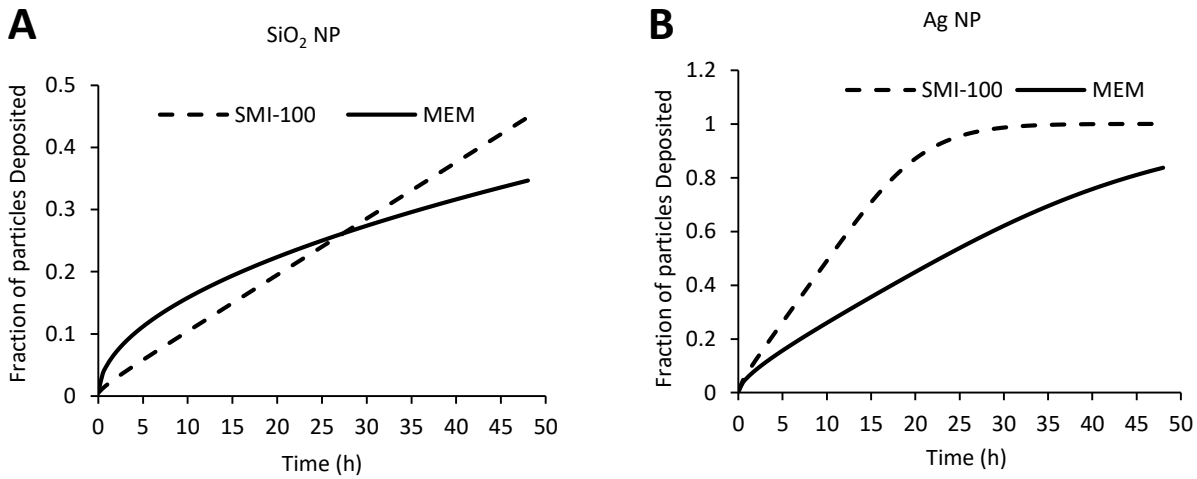

Figure 4. Dosimetric analysis of SiO_2, and Ag NPs in SMI-100 and MEM media. The NPs were sonicated at their $DSE_{(CRIT)}$ and suspended in SMI-100 or MEM media at 1mg/ml followed by volumetric centrifugation. Using the volume of pellets, effective densities of the test NPs were determined for SMI-100 and MEM media. These values were used to determine the fraction of particles sedimented (fD) over different time points for (A) SiO_2 NPs and (B) Ag NPs.

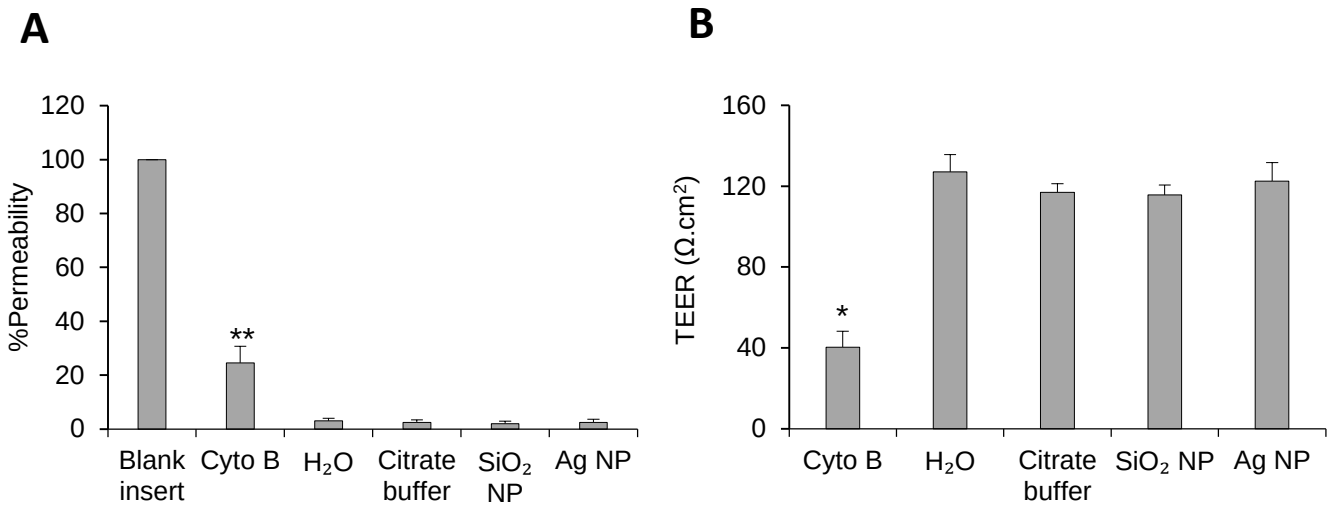

Figure 5. Measurement of barrier integrity after NP treatment. (A) FITC-dextran permeability assay and (B) TEER measurement of the 3D EpiIntestinal™ tissues treated with 50 µg/ml SiO_2 and Ag NPs apically for 72 hr. Cytochalasin B (20 µg/ml) was used as positive control. Water (10%) was the solvent control for SiO_2 NP and Cytochalasin B. Citrate buffer (5%) was the solvent control for Ag NP. Data were normalized against blank insert with extracelullar matrix before statistical analysis. Comparison of means was done using one-way ANOVA and Tukey's post hoc test: * $p < 0.05$, ** $p < 0.001$ compared with other sample groups in the corresponding series. Results from three independent experiments are shown, where each experiment consisted of a single microtissue per test dose. Values are presented as mean ± SD.

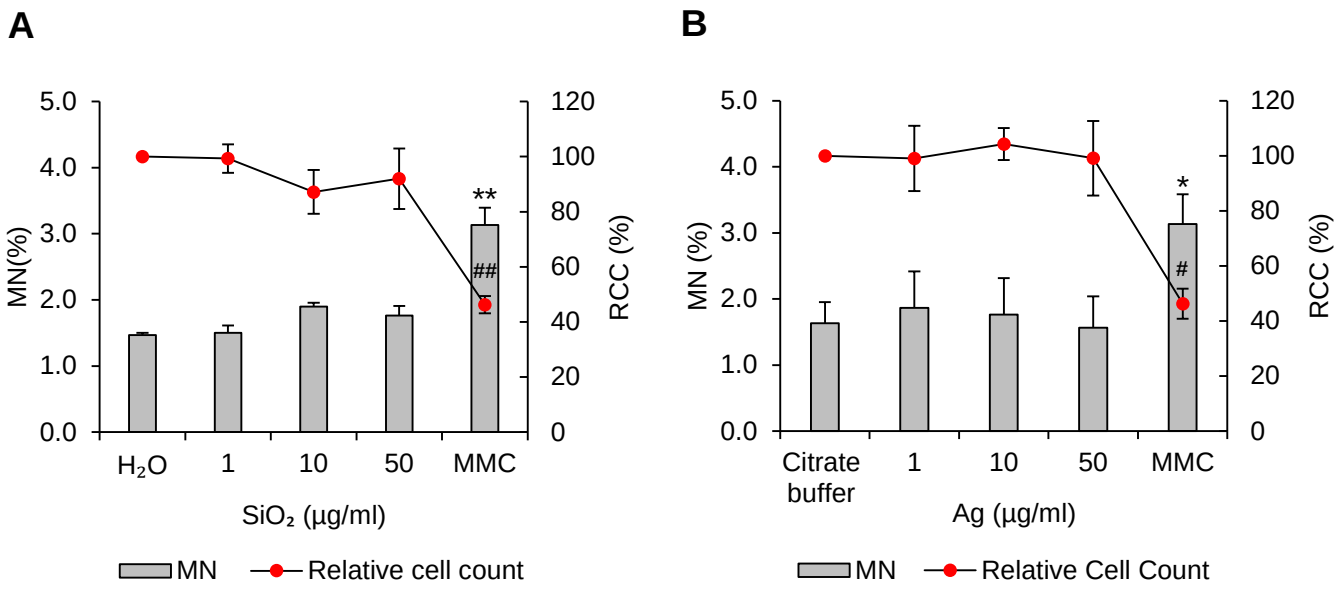

Figure 6. Micronuclei cytome genotoxicity assessment in 3D EpiIntestinal™ tissue. Tissues were exposed to test articles: (A) SiO_2 and B) Ag NPs for 10 days via apical treatment. At the end of treatment, tissues were dissociated to single cells and fixed in Carnoy's fixative scored according to the criteria described in Materials and Methods. One thousand total cells were scored per microtissue to determine the frequency of micronuclei (MN) induction and plotted together with RCC data. Mitomycin C (1 µg/ml) was used as positive control in 3D EpiIntestinal™ tissue. Water (10%) was the solvent control for SiO_2 NP. Citrate buffer (5%) was solvent control for Ag NP. Comparison of means was done using one-way ANOVA and Tukey's post hoc test: * $p < 0.05$, ** $p < 0.001$ compared with other MN % sample groups in the corresponding series; $^{\#}$ $p < 0.01$, $^{\#\#}$ $p < 0.001$ compared with other RCC % sample groups in the corresponding series. Values are presented as mean ± SD.

Figure 7

Click here to access/download;Figure;Figure_7.pptx

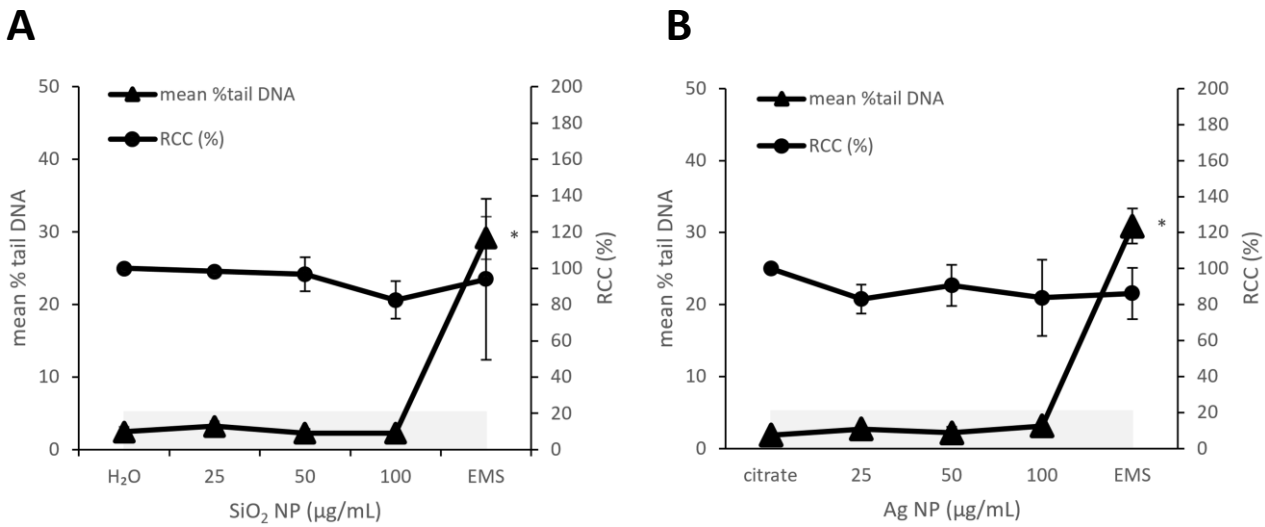

Figure 7. Comet genotoxicity assessment of NPs in 3D EpiIntestinal™ tissue. Tissues were exposed to test articles: (A) SiO_2, and (B) Ag NPs for 2 days via apical treatment. At the end of treatment, tissues were dissociated to single cells for comet slide preparation. One hundred viable comets were scored per microtissue to determine the median % tail DNA and plotted together with relative cell count (RCC %) data. The mean % tail DNA from three independent experiments are shown. Each experiment consisted of a single microtissue per test condition. Water (10%) and citrate buffer (10%) were solvent controls. Ethylmethanesulfonate (EMS) 500 µg/mL was used as the positive control. Comparison of means was done using one-way ANOVA and Tukey's post hoc test: * $p < 0.01$ compared with all other corresponding sample groups. Shaded area represents historical negative control range for %tail DNA where upper limit is 5.16%.

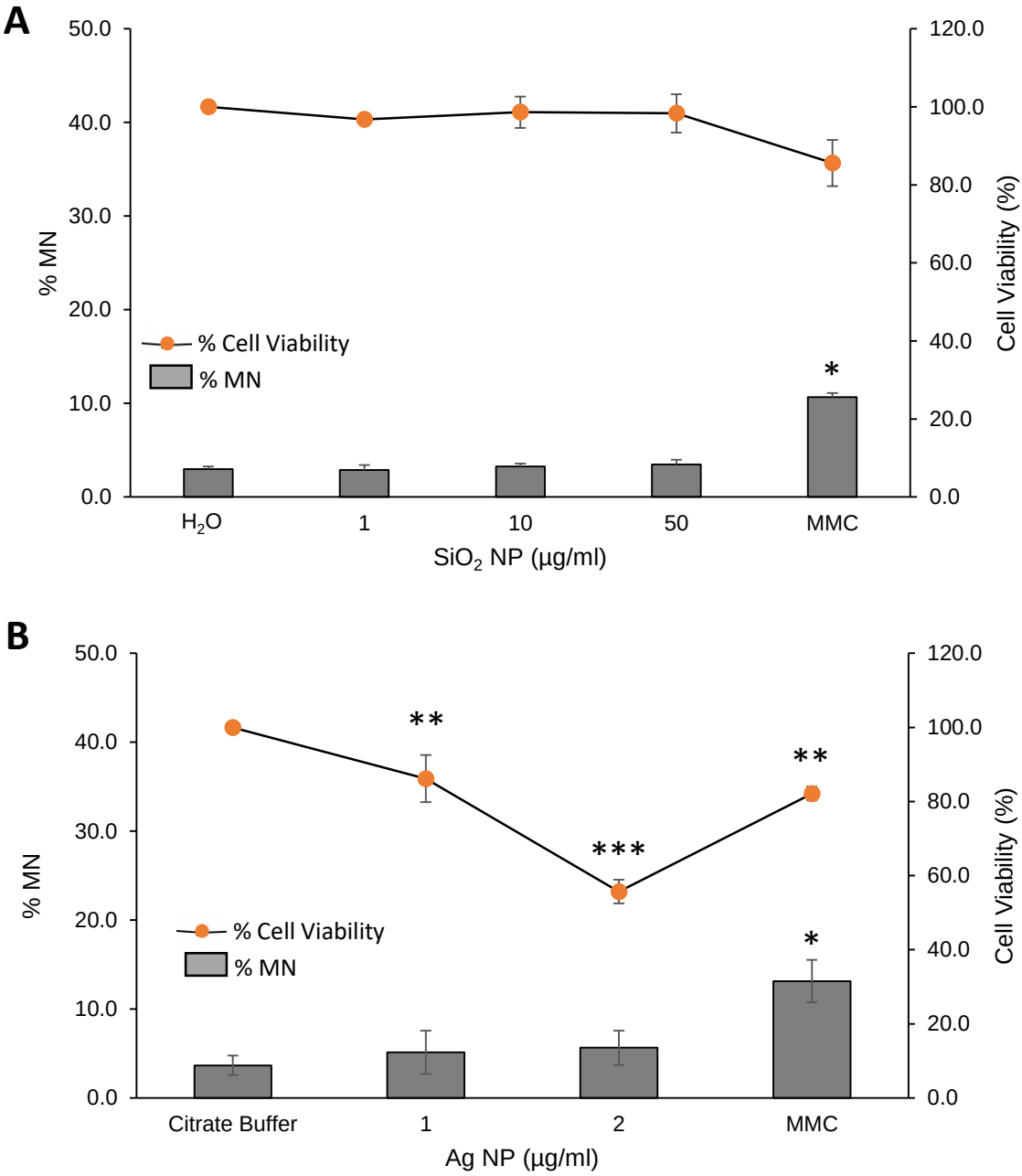

Figure 8. Micronuclei genotoxicity assessment in 2D Caco-2 gut cell line. Caco-2 cells were exposed to test articles: A. SiO_2, and B. Ag NPs for 24 hours. At the end of the treatment, cells were harvested by trypsin and fixed in Carnoy's fixative scored according to the criteria described in Materials and Methods. One thousand total cells were scored per replicate to determine the frequency of micronuclei (MN) induction. The results from three independent experiments are shown. Mitomycin C (0.03 µg/ml) were used as positive control. Water (10%) and citrate buffer (10%) were solvent controls. The values are expressed as percentages compared to solvent controls and presented as mean ± SD. Comparison of means was done using one-way ANOVA and Tukey's post hoc test: * $p < 0.05$ compared with other MN % sample groups in the corresponding series; ** $p < 0.01$, *** $p < 0.0001$ compared with solvent control.

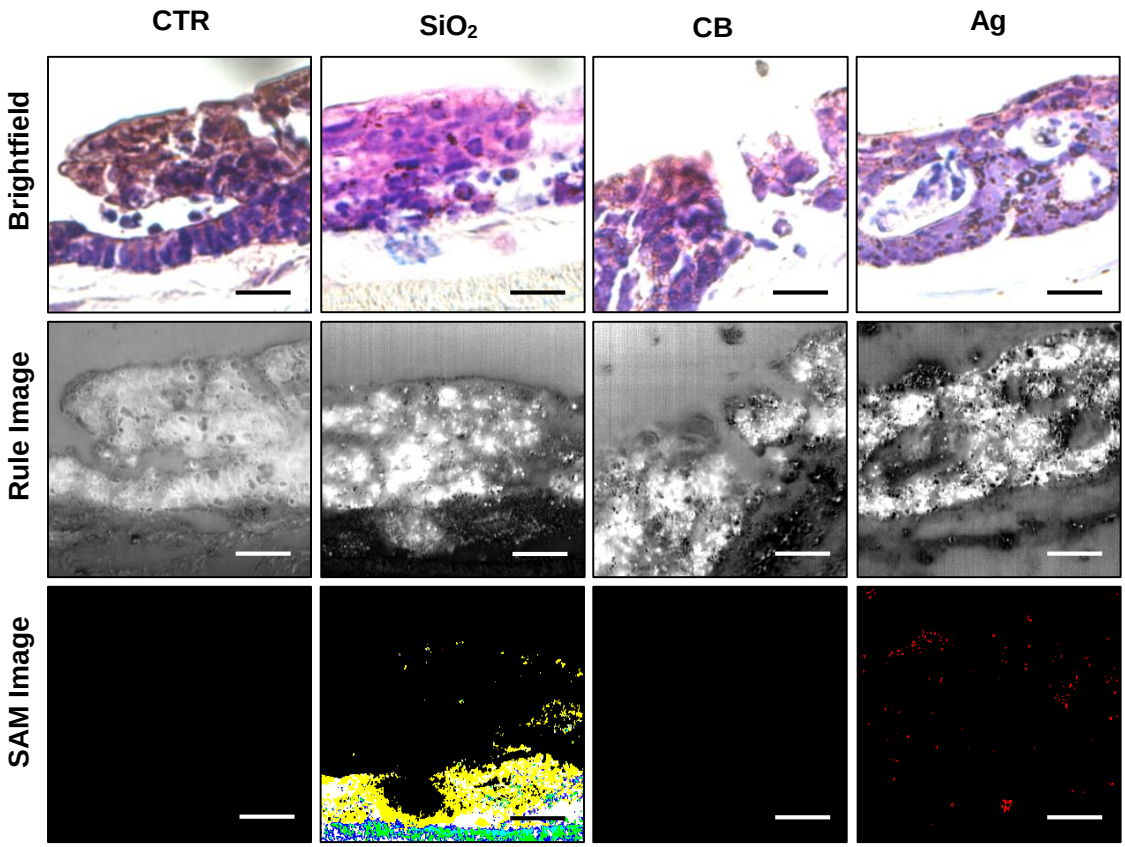

Figure 9. Hyperspectral imaging of 3D EpiIntestinal™ tissue. Tissues were either untreated (CTR) or administered with SiO_2 NPs, CB (Citrate Buffer) or Ag NPs and imaged under brightfield or darkfield conditions followed by spectral angle mapping to identify the NPs. Scale bars represent 20 µm.

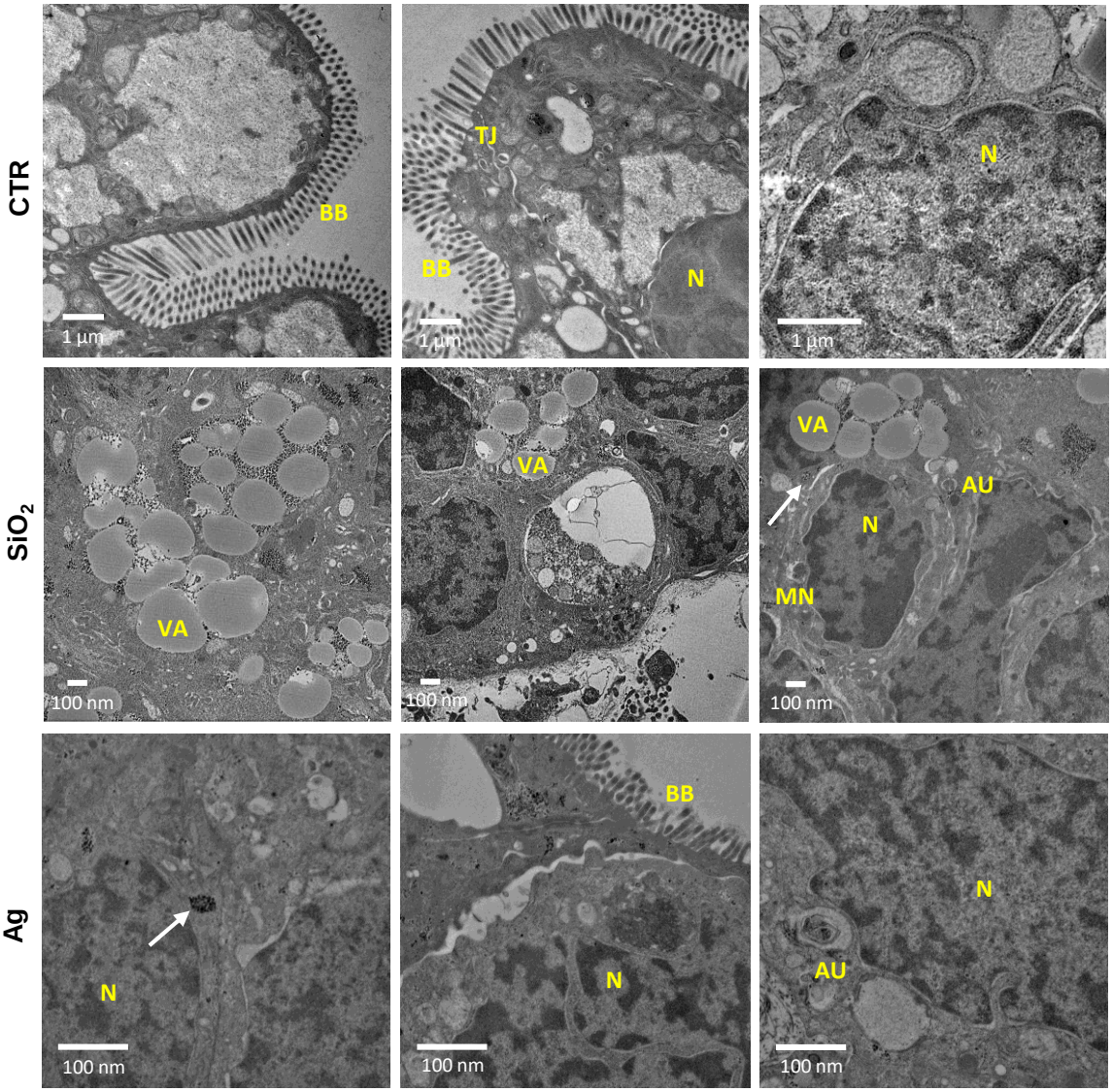

Figure 10. Transmission electron microscopy analysis. Representative TEM images of untreated controls (CTR), SiO_2 NPs and Ag NPs treated 3D EpiIntestinal™ tissues. The controls exhibited well-preserved organelle morphology. In contrast NPs treated cells displayed enlarged vacuoles, autophagosomes formation and presence of NPs within cellular compartments. N: Nucleus, BB: Brush borders, TJ: Tight junctions, AU: Autophagosomes, MN: Micronucleus, VA: Vacuoles. NPs are marked by white arrows.

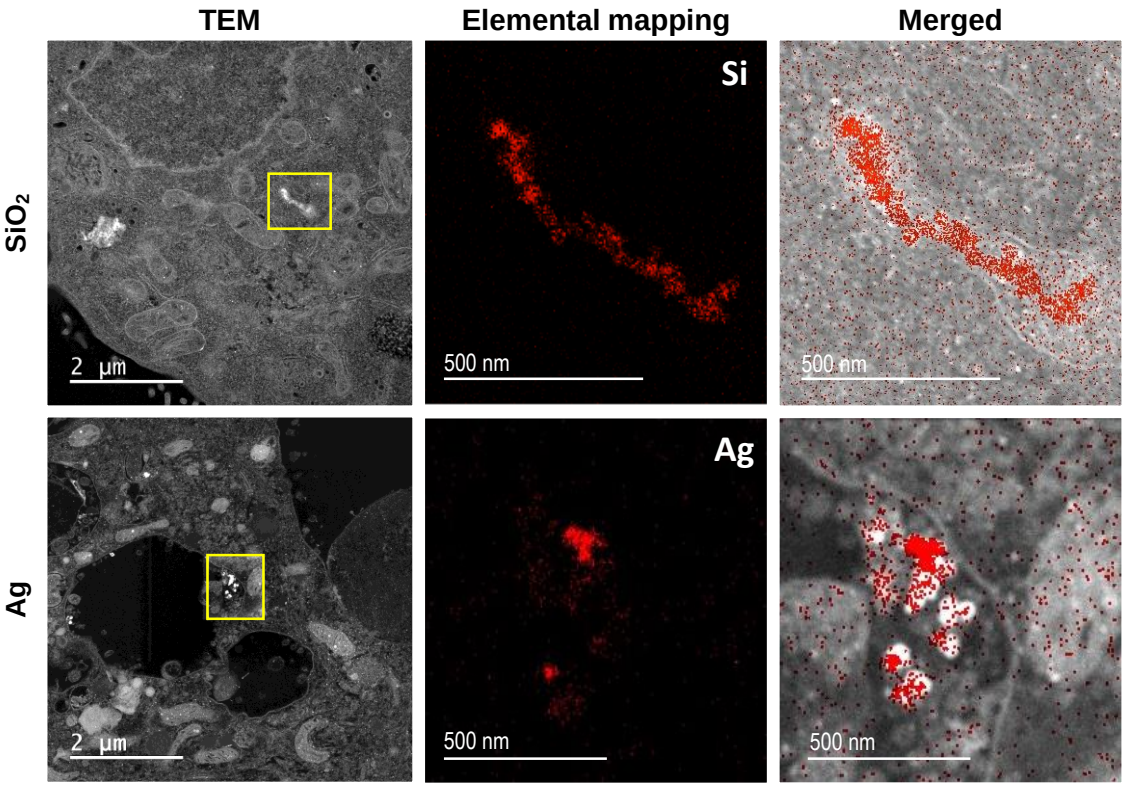

Figure 12. Scanning-Transmission Electron Microscopy with elemental mapping. TEM images merged with elemental mapping confirmed the uptake of SiO_2 and Ag NPs by Caco-2 cells. Yellow box = mapped area.

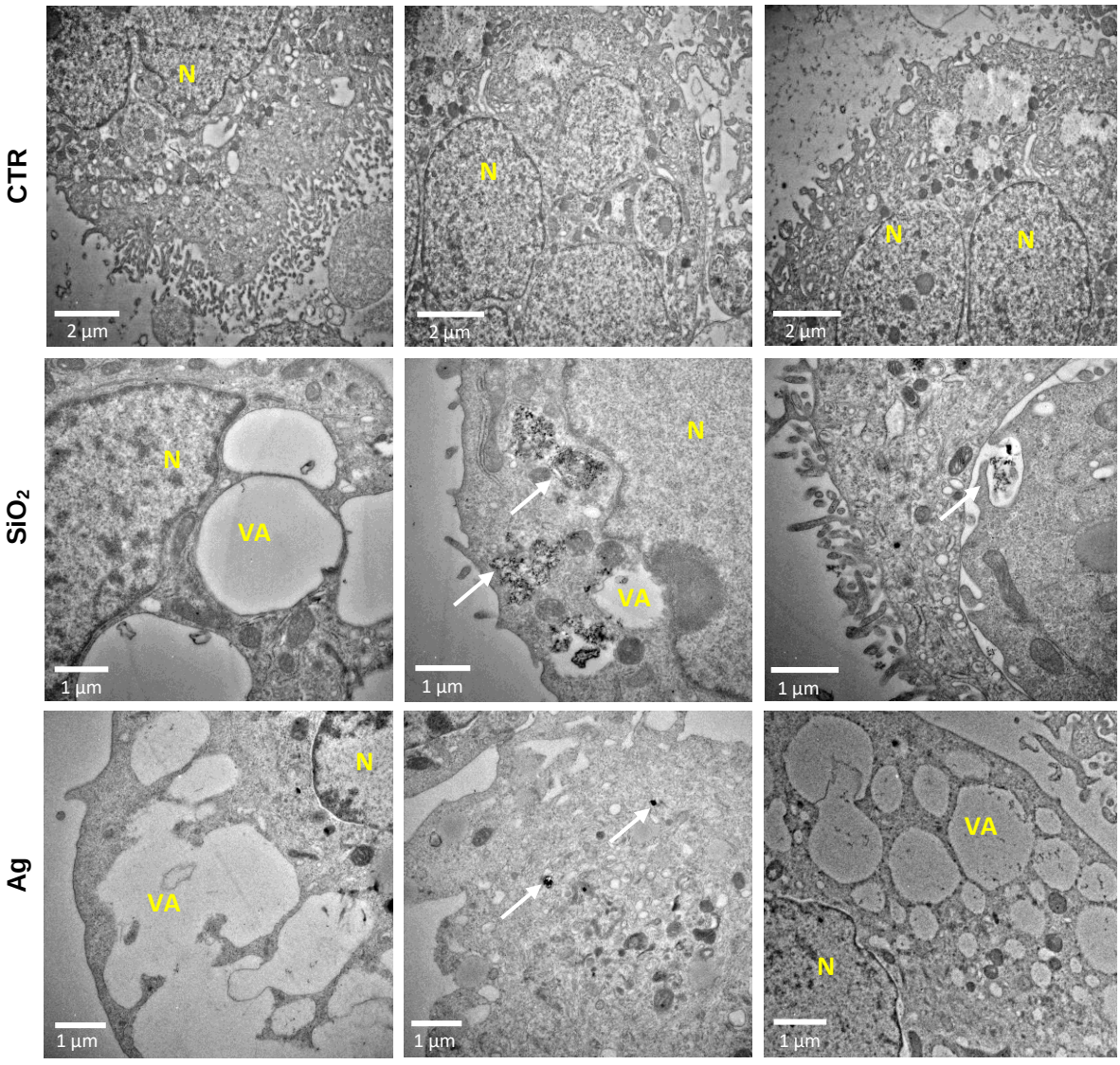

Figure 11. Transmission electron microscopy analysis on 2D cell cultures. Representative TEM images of untreated control (CTR), SiO_2 NPs and Ag NPs treated Caco-2 cells. The controls exhibited well-preserved organelle morphology. In contrast NPs treated cells displayed enlarged vacuoles, autophagosomes formation and presence of NPs within cellular compartments. N: Nucleus, VA: Vacuoles; NPs are marked by white arrows.

Assessing nanotoxicity of food-relevant particles: A comparative analysis of cellular responses in cell monolayers versus 3D gut epithelial cultures

Archana Gautam[1 #], Hui Kheng Lim[2,3,4 #], Jasmine Jia'En Li[5 #], Christopher Owen Hughes[2,3,4], Calvin Wee Sing Yeo[5], Moumita Rakshit[1], David Ian Leavesley[3], Michelle Jing Sin Lim[4,6], Joseph Choon Wee Tan[4], Li Yi Tan[1], Joanne Sheot Harn Chan[5], Benjamin Paul Chapman Smith[2,4,6,7 *], Kee Woei Ng[1,3,8 **]

Abstract

Engineered nanoparticles (NPs) are extensively used in the food industry, yet safety concerns remain. The lack of validated methodologies is a bottleneck towards resolving this uncertainty. Hence, the current study aims to compare two cell models by examining the toxicological impacts of two food-relevant NPs (SiO_2 and Ag) on intestinal epithelia using monolayer Caco-2 cells and full-thickness 3D tissue models of human small intestines (EpiIntestinal™). Comprehensive characterization and dosimetric analysis of the NPs were performed to determine effective doses and model realistic exposures. Neither genotoxicity nor cytotoxicity were detected in the 3D tissues after NP treatment, while the 2D cultures exhibited cytotoxic response from Ag NP treatment for 24 hr at 1 μg/ml. Hyperspectral imaging and transmission electron microscopy confirmed uptake of both NPs by cells in both 2D and 3D culture models. Ag NPs caused an increase in autophagy, whereas SiO_2 NPs induced increased cytoplasmic vacuolization. Based on realistic exposure levels studied, the 3D small intestinal tissue model was found to be more resilient to NP treatment compared to 2D cell monolayers. This comparative approach towards toxicological assessment of food relevant

NPs could be used as a framework for future analysis of NP behavior and nanotoxicity in the gut.